ANDERSON, WILLIAM EDWARD

DETERMINATION OF HYDROXYL RADICAL CONCENTRATION PROFILES IN THE LAMINAR, OPPOSED-JET DIFFUSION FLAME

THE UNIVERSITY OF ARIZONA M.S. 1984

DETERMINATION OF HYDROXYL RADICAL CONCENTRATION PROFILES IN THE LAMINAR, OPPOSED-JET DIFFUSION FLAME

by

William Edward Anderson

A Thesis Submitted to the Faculty of the

DEPARTMENT OF CHEMICAL ENGINEERING

In Partial Fulfillment of the Requirements
For the Degree of

MASTER OF SCIENCE

In the Graduate College

THE UNIVERSITY OF ARIZONA

1 9 8 4

STATEMENT BY AUTHOR

This thesis has been submitted in partial fulfillment of requirements for an advanced degree at The University of Arizona and is deposited in the University Library to be made available to borrowers under rules of the library.

Brief quotations from this thesis are allowable without special permission, provided that accurate acknowledgment of source is made. Requests for permission for extended quotation from or reproduction of this manuscript in whole or in part may be granted by the head of the major department or the Dean of the Graduate College when in his or her judgment the proposed use of the material is in the interests of scholarship. In all other instances, however, permission must be obtained from the author.

SIGNED: William Edward Anderson

APPROVAL BY THESIS DIRECTOR

This thesis has been approved on the date shown below:

J. O. L. WENDT
Professor of Chemical Engineering

11/28/84
Date

ACKNOWLEDGMENTS

A number of people were instrumental in the successful completion of this thesis. Thanks are in order at this time.

Firstly, many thanks and a great deal of respect to my major advisor, Professor Jost Wendt, who guided me through the project, contributed technical insight to the project, and also contributed to my own personal growth. Thanks also to other members of the Chemical Engineering faculty, especially Professors Peterson, Shadman, and Patterson, for their help in my graduate career and constructive criticisms of this thesis.

Mr. Sal Gonzales of the College of Mines Electronic Shop and Mr. Dick Van Reeth of the College of Mines Machine Shop provided invaluable help throughout the course of this project. Their patience and willingness to help was greatly appreciated, as well as their highly skilled work. Thanks also to Mrs. Rhoda Miller for her inimitable handling of administrative matters, and to Ms. Candice Corley for her expert help in the typing and final processing of this thesis.

Thanks to Mr. Tim Corley and Mr. Dan Lyons, partners in crime and at lunch, for a tremendous amount of help, friendship, and memories which will not soon be forgotten.

Finally, thanks to my wife, Christina, who made everything easier than it actually was, and to whom this thesis is dedicated.

TABLE OF CONTENTS

TABLE OF CONTENTS -- Continued

LIST OF ILLUSTRATIONS

LIST OF ILLUSTRATIONS -- Continued

LIST OF TABLES

ABSTRACT

The concentration profile of the OH radical in a $CO/H_2/He$ vs. O_2/He, laminar, opposed-jet diffusion flame was determined. Molecular absorption spectroscopy was used to study the $Q_1(2)$ through $Q_1(6)$ transitions of the (0,0) vibrational band in the ultraviolet system of OH. Peak absorptions of 5 to 15 percent were obtained with the 10-cm optical path length, resulting in calculated OH concentrations of 486 ppm at the lower limit of detection, to 1600 ppm at a plane in the flame slightly towards the oxidant side. The experimental results compare favorably with results from a computer simulation of a similar flame. Recommendations on improving the detection system are also made.

CHAPTER 1

PURPOSE AND SCOPE

Combustion systems, by nature, contain highly reactive chemical species such as H, OH, and O. These species are definitive in their effect on flame chemistry; in their absence, combustion of a fuel is not possible. In order to more completely understand the fundamental chemical kinetic processes occurring in a flame, experimentally derived quantification of as many of these species as possible is desirable.

The radical species H, OH, and O are the most important examples of transient species. Radical species are commonly defined as having one or more unpaired electrons. They are formed in excess of equilibrium in the active combustion regions of the flame and diffuse into cooler regions where their high reactivity is used to initiate and propagate combustion.

These transient species generally have lifetimes of milliseconds or less. Thus, they may not be extractively sampled, but must be measured in situ. Spectroscopic methods have proven to be ideal in such applications. OH may be quantitatively determined by the well-known and straightforward procedure of absorption spectroscopy. The OH radical is of major importance as an oxidizing species and much spectroscopic data has been compiled on it.

Spectroscopy is the study of the interaction of electromagnetic radiation with matter. In molecular absorption spectroscopy, radiant energy in the form of light is absorbed by a molecule. If molecular spectroscopic properties are known, the number of absorbers may be calculated from the measured attenuation of light due to absorption at a given wavelength.

The laminar, opposed-jet diffusion flame (Hahn and Wendt, 1981; Corley, 1984) is in use in our laboratory as a tool for studying high-temperature, atmospheric-pressure, physical and chemical processes occurring in flames. The flame (Figure 1.1) is one-dimensional in temperature, concentration, and reaction rates; and two-dimensional in radial velocity and pressure. It has advantages over premixed flames in that it consists of fuel-rich and fuel-lean zones of varying extents, it is suspended in space and free from direct burner surface heat loss and catalytic effects, and it is amenable to rigorous mathematical analysis. The opposed-jet configuration affords a flame which may be considered as a prototype model for laminar flamelets in turbulent diffusion flames. Its detailed structure has been modeled by coupling of the momentum and energy conservation equations, using detailed finite-rate combustion kinetics.

The current focus of research in progress is on the mechanisms of formation of the primary pollutant NO from chemically bound nitrogen in fuel. The overall scheme of the fate of fuel nitrogen is widely accepted; however, the detailed mechanisms are a subject of considerable

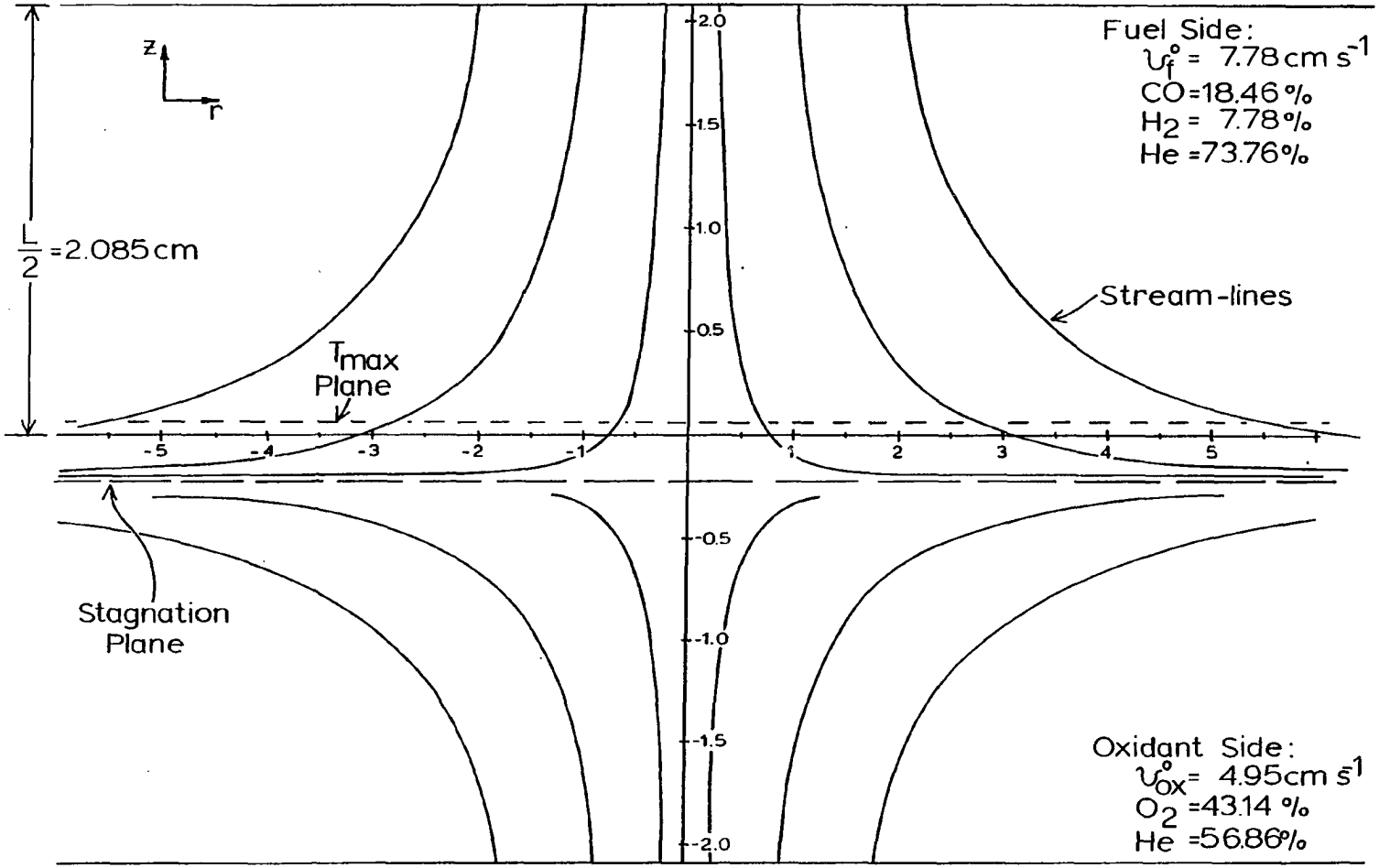

Figure 1.1 Laminar, opposed-jet diffusion flame.

controversy. Experimental determination of [OH] will aid in the elucidation of the overall mechanism.

The kinetic mechanisms of fuel nitrogen pyrolysis in very fuel-rich environments may be the controlling factor in fuel NO formation. The opposed-jet flame, by virtue of its well-defined division of fuel-rich and fuel-lean zones, is an ideal system in which to study fuel-rich kinetics.

Prior to this work, capability existed for the determination of stable species concentration profiles by extractive sampling and analysis, and temperature profiles by thermocouple measurements. Knowledge of transient species concentration profiles would lead to better predictability and greater accuracy of the model.

The objectives of this project were: 1) to explore current techniques and furnish the laboratory with a knowledge of equipment, practical expertise, and theory; 2) to design a low-cost system for the optical detection of transient species; 3) to implement this system, in conjunction with the existing experimental system, for the determination of OH radical concentrations in the laminar, opposed-jet diffusion flame being studied in the laboratory; and 4) to make recommendations regarding future work in this area.

CHAPTER 2

BACKGROUND

2.1 Chemistry of Free Radicals

High-temperature chain reactions, in which free radicals take part, are classified as: 1) initiation reactions with high energies of activation, in which radicals are formed; 2) chain-branching reactions, in which combination of a radical with a stable species produces two chemically reactive species; 3) chain-propagation reactions, in which a radical and a stable species combine to form a different pair of species, one stable and one unstable; and 4) chain-termination reactions, in which the unstable species react to form stable species. These steps are detailed as follows:

1. Chain initiation:

$$H_2O + M \rightarrow OH + H + M \qquad \text{(R 2.1)}$$

$$O_2 + M \rightarrow O + O + M \qquad \text{(R 2.2)}$$

2. Chain branching:

$$O_2 + H \rightleftarrows OH + O \qquad \text{(R 2.3)}$$

$$H_2 + O \rightleftarrows OH + H \qquad \text{(R 2.4)}$$

$$H_2O + O \rightleftarrows OH + OH \qquad \text{(R 2.5)}$$

3. Chain propagation:

$$H_2 + OH \rightleftarrows H + H_2O \qquad \text{(R 2.6)}$$

4. Chain termination:

$$OH + H + M \rightarrow H_2O + M \qquad \text{(R 2.7)}$$

$$O + O + M \rightarrow O_2 + M \qquad \text{(R 2.8)}$$

$$H + H + M \rightarrow H_2 + M \qquad \text{(R 2.9)}$$

In the above reactions, M is a "third-body" species which acts to absorb (or give up) energy.

The free radical species H, OH, and O are prevalent in many dominant fundamental reactions occurring in the flame. Under certain conditions, knowledge of the concentration of one of the radical species, along with knowledge of concentrations of appropriate stable species, may lead to an approximation of one or both of the other free radical concentrations. For example, in Kaskan's (1959) study of premixed $H_2/O_2/N_2$ flames, he assumed rapid bimolecular reactions (R 2.3-R 2.6) to be locally equilibrated, and deduced the concentrations of O_2, O, and H from measured H_2, H_2O, and OH, and known equilibrium constants. Use of the partial equilibrium assumption (e.g., Glassman, 1977) resulted in proportionalities between [O] and $[OH]^2$, [H] and [OH], and $[O_2]$ and $[OH]^2$.

The above is an example of the use to which a known OH concentration may be put. It may also be used to find rate constants which are not certainly known. Given a postulated reaction mechanism, it may be used to determine which reactions are dominant, or even feasible. It may also result in the calculation of the concentration of another species taking part in reactions which OH does not participate in, thereby giving information on reactions in which the unknown is taking part.

2.2 Flame Chemistry of Nitrogen Oxide

Nitrogen oxide is formed during combustion from two sources: atmospheric nitrogen and fuel nitrogen. The chemistry of nitrogen oxide formed under fuel-lean and stoichiometric conditions by reaction of atmospheric nitrogen is well-known. The kinetics in this case are governed by the Zeldovich (1946) mechanism:

$$O + N_2 \rightarrow NO + N \qquad \text{(R 2.10)}$$

$$N + O_2 \rightarrow NO + O \qquad \text{(R 2.11)}$$

It is thought to be the main source of NO in most combustion systems. In this case, NO is formed in the post-flame zone, as reaction (R 2.10) has a high energy of activation. For this reason, it is termed "thermal NO."

Fenimore (1971) postulated that NO is also formed in the flame zone of hydrocarbon flames, and termed this NO "prompt NO." Fenimore thought it was formed through stable cyanide intermediates formed from hydrocarbon radicals, as:

$$CH + N_2 \rightarrow HCN + N \qquad \text{(R 2.12)}$$

N would subsequently be oxidized, primarily by OH, in the post-flame region to form NO.

Morley (1976), using a mass spectrometer to measure HCN, NH_3, and NO in fuel-rich flames, determined that HCN was the dominant nitrogenous species leaving the primary reaction zone, regardless of whether the source of nitrogen was fuel or atmospheric. He also showed that the HCN measured in the reaction zone corresponded to the concentration of prompt NO measured downstream.

The superficial reaction mechanism for fuel nitrogen is generally accepted as:

$$\text{fuel-N} \rightarrow \text{HCN} \rightarrow \text{NH}_i \begin{cases} \rightarrow \text{NO} \\ \rightarrow \text{N}_2 \end{cases} \qquad \text{(R 2.13)}$$

where NH_i is either N, NH, NH_2, or NH_3. However, there is still much debate on the detailed reaction scheme. Fenimore (1976), Morley (1976), and Haynes (1977a, 1977b) discuss postulated mechanisms and their own preferences, but the fundamental reactions in the conversion of fuel nitrogen to NO and N_2 under fuel-rich conditions still must be considered to be in doubt. A simplified reaction scheme for this system is given in Figure 2.1. As may be expected, the radicals H, OH, and O are prevalent in the fundamental reactions. Obviously, experimentally measured OH would help clarify the situation.

The laminar, opposed-jet configuration, with its well-defined fuel-rich zone, affords the type of analysis necessary for the determination of the fate of fuel nitrogen at its earliest stages.

2.3 Previous Literature on Absorption by OH in Flames

Due to the importance of OH in flame kinetics, its ultraviolet bands, which correspond to the transition of OH from its lowest electronic state to its first excited electronic state, have been extensively studied. All information about them has been compiled by Dieke and Crosswhite (1962), who made accurate measurements of the over 1,500 spectral lines emitted by the outer cone of an acetylene-oxygen flame, and calculated all band constants. Their report contains:

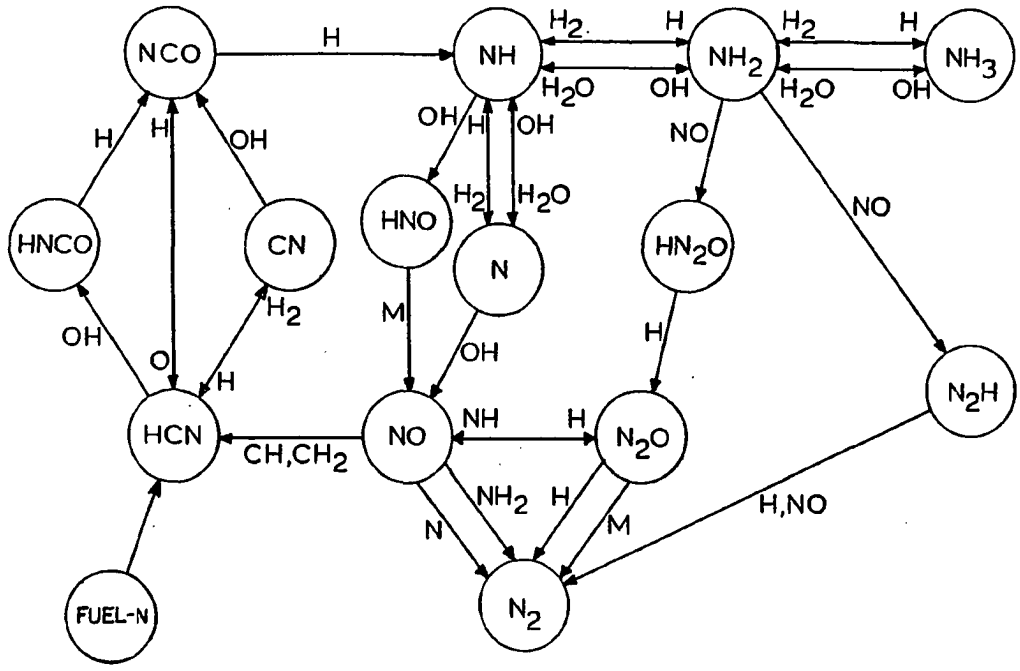

Figure 2.1 Simplified reaction scheme for conversion of fuel nitrogen to nitrogen oxide. -- From Corley (1984).

1. A wavelength table of lines between 2811 Å and 3546 Å, listed by increasing wavelength, intensity, and notation.
2. A wavelength table of the same lines listed by bands.
3. A table of the spectral terms up to N = 32 for some bands, listed by vibrational levels v = 0, 1, 2, and 3 for both lower and upper electronic states.
4. A table of transition probabilities and application of the iso-intensity method for spectroscopic determination of temperature.
5. The values of the molecular constants of both electronic states.
6. An extensive set of references.

Early spectroscopic studies of flames were done by studying the spectra of emitting atoms and molecules using a photographic emulsion to determine the wavelength dependency of emission of radiation. One of the first examples of using absorption spectroscopy in the study of OH radicals in flames was by Kostowski and Broida (1956). However, the focus of their work was on the determination of the temperature of the hot gases.

One of the problems facing early researchers in this area was the design of burners amenable to spectroscopic studies (Gaydon and Wolfhard, 1948). Stable flames on premixed burners were too optically thin for study, except for instruments with very high resolving power. Also, flames were three-dimensional, and it was not possible to determine the exact location of the emitters or absorbers. A mathematical method to deal with the latter problem is discussed later in this thesis.

Wolfhard and Parker (1949) overcame these difficulties by construction of a flat, two-dimensional diffusion flame with optical depth of 5 cm and a reaction zone 5-10 mm thick. Their first study on the subject, a study of the intensity of emission and absorption in an H_2/O_2 flame determined by exposure of a photographic emulsion, provided a qualitative view of the concentration of OH in the flame. Maximum concentration of OH occurred coincidentally with maximum temperature. No attempt was made to quantify this concentration.

In a subsequent study on the flat diffusion flame, Wolfhard and Parker (1952) quantified OH concentrations in various flames. The strength of absorption, as indicated by photographic exposure, was calibrated in terms of OH concentration by use of a premixed flat flame of similar geometry. They calculated the OH concentration corresponding to its chemical equilibrium concentration in a region 1-2 mm above the inner cone of the premixed flame, where the temperature reaches the theoretical flame temperature corresponding to the mixture strength. A calibration curve was obtained by varying the stoichiometry of the flame from fuel-rich to stoichiometric, which results in a steep rise of OH towards the stoichiometric region. In their study, Wolfhard and Parker assumed the population of OH in various vibrational and rotational levels was constant over the range of temperatures (2500-3000 K) they encountered in their flames. They also assumed the factors contributing to the broadening of the absorption lines had negligible dependence on temperature. Maximum OH concentrations occurred slightly to the fuel-lean side of the maximum temperature.

Kaskan (1957) developed a cooled, porous metal burner, which provided a flat, one-dimensional, stable, premixed flame. Flame temperatures were determined by amount of cooling provided. Kaskan utilized the line absorption method, whereby the source of background radiation is the emission of OH in water vapor stimulated by a D.C. discharge of approximately 30 ma. This method provides narrow emission lines, which are then absorbed by the broader absorption lines at their line center. This method results in an easier analysis. The burner diameter in this study was 4.7 cm. Kaskan used a multipass optical scheme, to increase optical depth, for lines which showed weak absorption. For H_2/O_2 flames, Kaskan found that the OH concentration occurring near the flame zone was greatly in excess of equilibrium values, ranging from typical factors of 1000 for fuel-rich flames to about 50 for fuel-lean flames.

Laud and Gaydon (1971) measured absorption of OH on flat, counterflow diffusion and Wolfhard-Parker type burners. Their counterflow flame is similar to the system in use in our laboratory. Burner separation of 1.2 cm gave the steadiest flat flame. The optical system consisted of a continuous source (150 W xenon arc lamp), a mechanical chopper, phase-sensitive detection used to discern signal from background noise (flame emission and electronic noise), a 0.5-m monochromator, and a photomultiplier tube. Details of analysis are sketchy. For an ethylene/oxygen flame with stoichiometric ratio 0.5, they report a maximum OH concentration of approximately 7×10^{15} molecules/cc, corresponding to about 15 percent peak absorption at a point slightly removed toward the oxygen side from the point of maximum temperature.

Bulewicz, Padley, and Smith (1970) determined the temperatures and concentrations of OH, CH, and C_2 in a premixed flame. The optical system consisted of a continuous source, mechanical chopper, 1-m monochromator, photomultiplier tube, and phase-sensitive detection. All three diatomic species were evident in absorption, although it was necessary to increase the optical path length to 3.6 m to increase the absorption by C_2 and CH to above 5 percent, which corresponded to concentrations of about 10^{11}-10^{12} molecules/cc. C_2 and CH were found to be in excess of equilibrium by several orders of magnitude in the flame zone.

Schmidt and Malte (1976) studied the absorption of OH occurring in a turbulent, jet-stirred reactor. The optical system consisted of a continuous source, light chopper, sapphire windows for optical access to the reactor, and phase-sensitive detection. A multipass optical system was used to increase the depth of the 6-cm diameter reactor. The analysis of data in this report was rather rigorous, although, in the end, it was necessary to make some simplifying assumptions. Measurements of integrated absorption across resolved rotational lines resulted in calculated OH concentrations in the hydrogen/air and methane/air flames studied on the order of 10^{15} molecules/cc.

Certain conclusions may be drawn from these prior studies, and served as a guide for this study. The OH radical is easily studied in its ultraviolet electronic system utilizing the strongly absorbing (0,0) vibrational band of the electronic transition from its ground state to its first excited state at about 3100 Å. There are also other vibrational bands in this system observable in absorption.

This spectral region is free from transitions of other species which may occur in flames. Certain strongly absorbing lines in the rotational structure can be resolved by an instrument with moderate resolution, i.e., the monochromator presently in use in our laboratory.

A xenon arc lamp is a suitable choice for the background radiation source. A premixed flame, in which one can reasonably calculate *a priori* OH concentration as a function of temperature and reactant mixture, can serve as a calibrating source. In this study, a premixed flame served as a means of checking the experimental set-up.

For a reasonable path length (the opposed-jet burner diameter of 10 cm is definitely reasonable), an OH concentration of approximately 10^{15} molecules/cc results in at least 5 percent maximum absorption in certain absorption lines. This concentration exists in most flames at near stoichiometric conditions. A maximum absorption of 10-15 percent is desirable, as this results in considerable simplification in treatment of data, i.e., the Beer-Lambert law may be used. Individual absorption lines to be studied must be at least 1.0 Å removed from each other to resolve the lines with the monochromator in use. This is due to the necessity of opening the slits of the monochromator wide enough to maintain a reasonable signal-to-noise ratio.

2.4 Other Spectroscopic Methods

Two relatively recent developments have revolutionized the art of spectroscopy: tunable lasers in the ultraviolet and visible regions, and high-resolution, two-dimensional array cameras. Most recent publications in spectroscopic studies of flames have utilized one or both of

these techniques. Combination of these techniques with large-scale computational techniques enables the researcher to make microscopically based studies of the extremely complex fundamental mechanisms in combustion chemistry possible. An extensive survey of laser techniques has been published by Crosley (1980).

CHAPTER 3

THEORY

3.1 Introduction to Spectroscopy

Spectroscopy is the study of the interaction between matter and electromagnetic radiation. In absorption, a photon of energy $h\nu$ is absorbed by a molecule in a particular quantum state of energy E". A transition to another state of higher energy E' is induced. In emission, electromagnetic radiation is emitted by a molecule undergoing a transition from a quantum state with energy E' to a state with energy E". Conservation of energy leads to the relation:

$$\Delta E = h\nu = E' - E'' = \frac{hc}{\lambda} \qquad (3.1)$$

where h = Planck's constant, 6.626×10^{-34} J-sec; ν = frequency, cm^{-1}; c = speed of light, 2.998×10^{10} cm-sec^{-1}; and λ = wavelength of radiation, cm.

In the transient diatomic molecules of interest in this study, energy may be considered to be absorbed in three modes: electronic, vibrational, and rotational. There are three types of spectra in correspondence with these modes: 1) rotational spectra, in which transitions take place from one rotational level to another while remaining in the same vibrational and electronic states; 2) rotation-vibration spectra, in which transitions take place from the rotational levels in a

given vibrational level to rotational levels of another vibrational level in the same electronic state; and 3) electronic spectra, in which transitions from the rotational levels of the various vibrational levels of a given electronic state take place to the rotational and vibrational levels of a higher electronic state. Figure 3.1 illustrates these concepts. Therefore, equation (3.1) may be written:

$$h\nu = (E'_{el}-E''_{el}) + (E'_{vib}-E''_{vib}) + (E'_{rot}-E''_{rot}) \qquad (3.2)$$

where

$$E'_{el}-E''_{el} >> E'_{vib}-E''_{vib} >> E'_{rot}-E''_{rot}$$

The magnitude of $h\nu$ absorbed or emitted is governed by the type of transition involved. The electronic transition from ground electronic state OH to its first excited state is studied here.

The electronic spectra of an acetylene/air flame is presented in Figure 3.2. The dominant feature is the vibrational band of OH centered around 3064 Å. This represents the (0,0) vibrational band, i.e., the transition occurs between vibrational states $v' = 0$ and $v'' = 0$. Within this band, fine structure which corresponds to changes in rotational states can be detected.

In order to interpret the discretization of energy, the diatomic molecule has been modeled as having the ability to attain only certain "stationary states" (e.g., Herzberg, 1971).

The wave function is considered to define the properties of a molecule. The wave function of a system of particles (nuclei in a molecule) is a function of their coordinates and represents a probability distribution of finding a molecule at those coordinates. An n particle

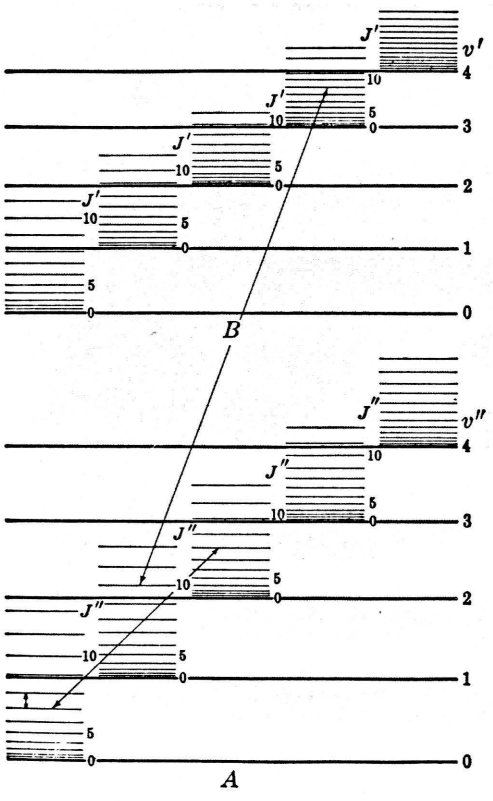

Figure 3.1 Vibrational and rotational levels of two electronic states, A and B. -- The three double arrows indicate examples of transitions in the pure rotation spectrum, the rotation-vibration spectrum, and the electronic spectrum of the molecule. From Herzberg (1971).

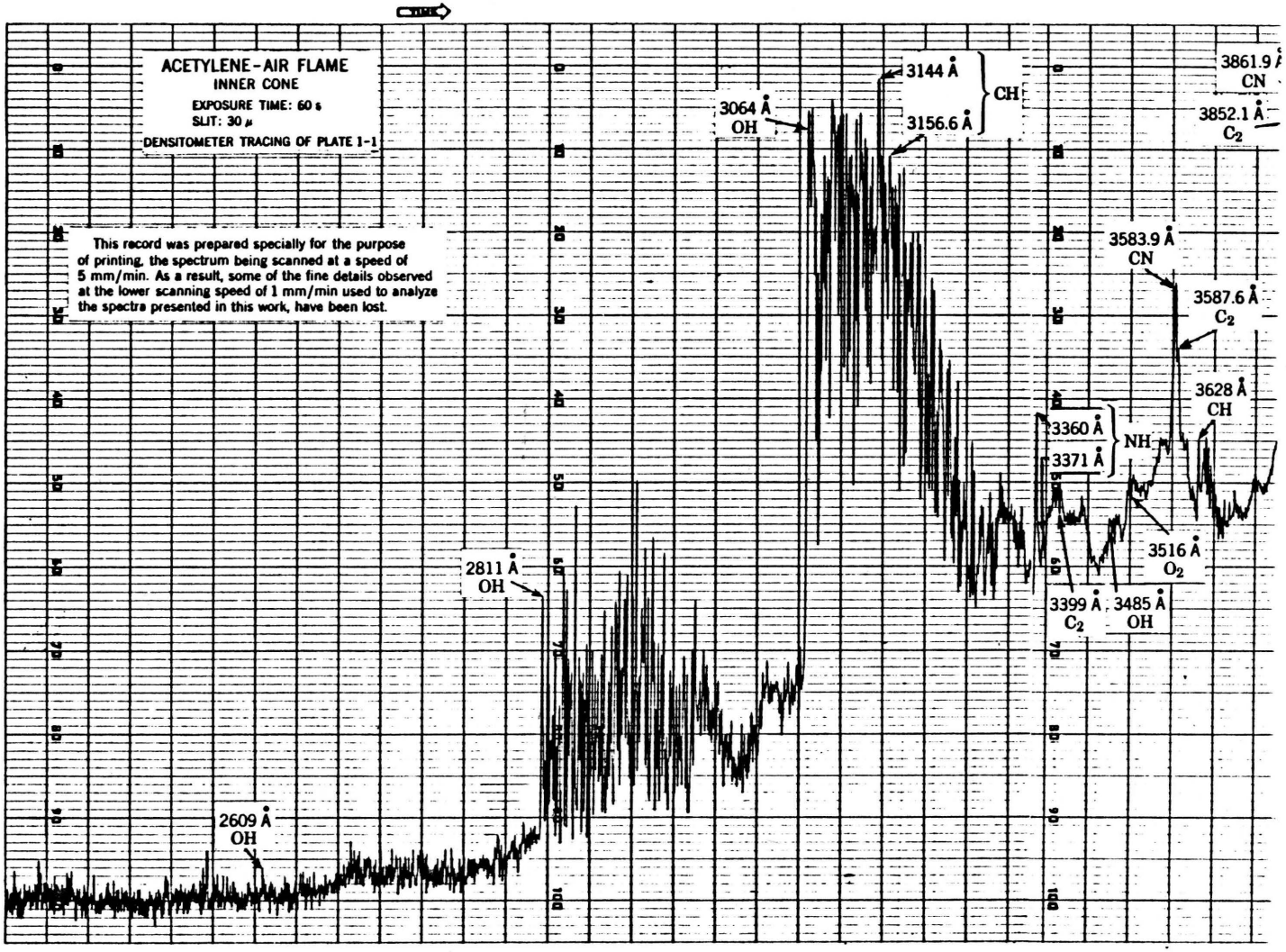

Figure 3.2 Electronic spectra in an acetylene/air flame.

system results in 3n coordinates. If the molecular electrons possess a spin, the spin coordinates also contribute. For the allowed quantum states of a molecule, the wave function is the solution of the Schrödinger equation for the model.

Since the energy of a molecule may be approximated as the sum of three energies, the wave function of a molecule may be considered as the product of three separate functions: 1) a function of the coordinates and spin of the molecular electrons only, 2) a function of the separation of the nuclei, and 3) a function of the angle of the straight line joining the nuclei with a fixed direction.

The state of a molecule is specified by a set of quantum numbers which describe the allowed vibrational, rotational, and electronic states of the molecule. Absorption or emission of radiation causes a change in the set of quantum numbers. Allowable changes in quantum states, governed by the so-called "selection rules," are given in terms of quantum numbers. The selection rules pertaining to these molecular transitions are given in any fundamental text on molecular spectroscopy, e.g., Herzberg (1971) and Steinfeld (1974).

The observed intensity of a transition obviously is dependent on the number of absorbers in the lower state of the transition in absorption, or on the number of emitters in the upper state of the transition in emission. The intensity of a transition is also dependent on on ν, the frequency at which the transition occurs, as defined by the Franck-Condon principle (Herzberg, 1971).

The basis of this principle is that, in an electronic transition, the quantum jump from one electronic state to the other is very

fast compared to the motion of the nuclei. During the electronic transition, the nuclei do not change their positions, and are now resident in quantum states with quantum numbers corresponding to the spatial coordinates of the nuclei in the new electronic state. In quantitative terms, transition probability depends on the "overlap" of the vibrational wave function of the initial and final states (see Figure 3.3).

In quantitative absorption spectroscopy, one or more of the wavelengths at which a transition occurs is monitored. Measurement of the attenuation of intensity of the background radiation source due to absorption at these wavelengths, combined with known spectroscopic constants of the molecule, will yield an equation for the calculation of the number of absorbers resident in the lower state of the transition.

The relative distribution of molecules within the rotational, vibrational, and electronic states as a function of temperature is governed by the Boltzmann distribution. Experimentally determined distributions give rise to the notion of spectroscopic temperatures, whereby the distribution is fit to Boltzmann statistics, yielding the temperature at which the populations are in thermal equilibrium.

3.2 Absorption Lines and Absorption Coefficient

When parallel light from a continuous source is passed through a medium containing atoms or molecules which have allowed energy transitions corresponding to frequency $\tilde{\nu}_0$, the intensity of the transmitted light has a frequency distribution as shown in Figure 3.4.

This gas, then, has an absorption line at frequency $\tilde{\nu}_0$. The absorption coefficient of the gas is defined by the equation:

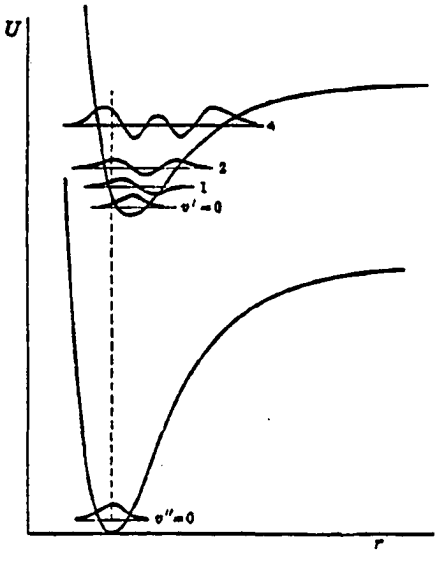

Figure 3.3 Potential curves and wave functions of the vibrational states explaining the wave-mechanical form of the Franck-Condon principle. -- The potential functions of the upper and lower states are assumed to have such a relative position that the best overlapping of the wave functions occurs for $v'' = 0$, $v' = 2$. From Herzberg (1971).

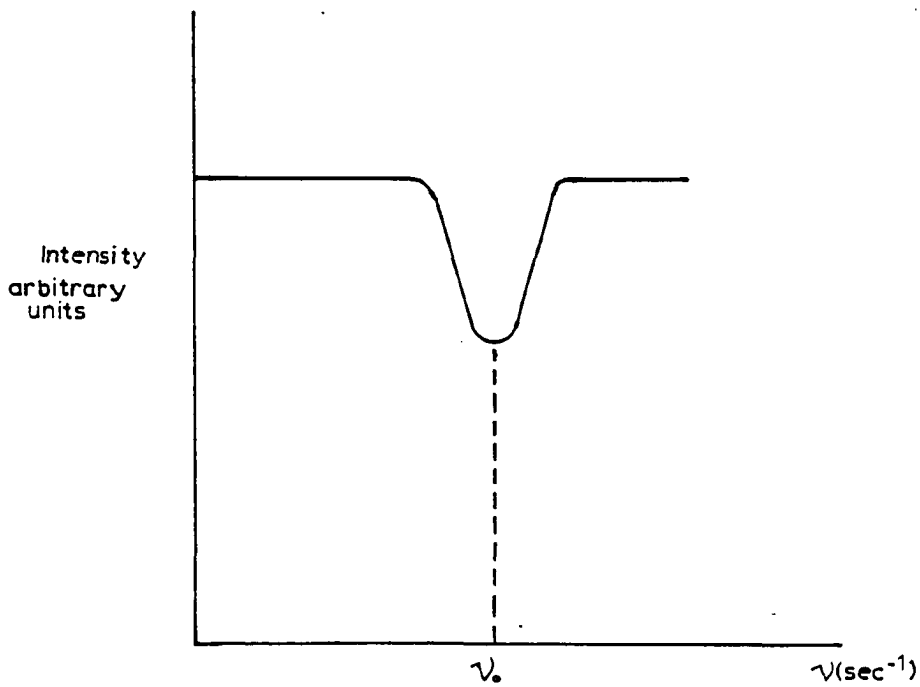

Figure 3.4 Frequency distribution of transmitted light.

$$I(\tilde{\nu}) = I_0(\tilde{\nu}) \exp [-k(\tilde{\nu})\ell] \qquad (3.3)$$

where ℓ (cm) is the optical depth of the gas. The absorption coefficient, $k(\tilde{\nu})$, depends on the properties of the absorbing gas and frequency $\tilde{\nu}$. The frequency dependency of $k(\tilde{\nu})$ is shown in Figure 3.5.

The distance between the two points on the curve at $k(\tilde{\nu}) = \frac{1}{2} k_{max}$ is defined as the half-width of the absorption line and is denoted as $\Delta\tilde{\nu}$. The integral of $k(\tilde{\nu})$ over the spectral range of the line is termed the integrated absorption, K:

$$K = \int_{line} k(\tilde{\nu}) d\tilde{\nu} \qquad (3.4)$$

and is proportional to the product of the number of absorbers in the lower state of the transition and the oscillator strength of the absorption line. The oscillator strength is related to the transition probability as discussed in the Franck-Condon principle. The relationship is:

$$K = \frac{\pi e^2}{mc^2} N_{J''} f_{12} = 2.653 \times 10^{-12} N_{J''} f_{12} \qquad (3.5)$$

where $N_{J''}$ is the number of absorbers in lower state J" (cm^{-3}); f_{12} is the absorption oscillator strength of the line; and m and c are the mass and charge of an electron, respectively.

As indicated by Figure 3.5, absorption lines show a definite width and shape. Only a dispersing instrument with infinite resolution could give the true shape of the line. Lines are generally characterized by their half-width, $\Delta\tilde{\nu}$.

The relevant phenomena at atmospheric pressure responsible for the width and shape of the absorption line are classified as follows:

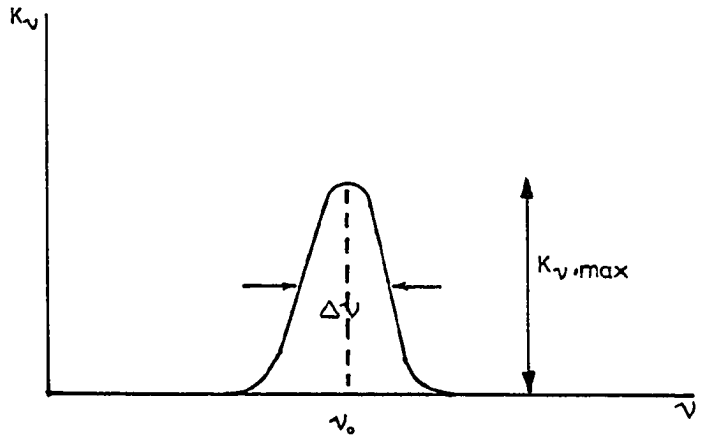

Figure 3.5 Frequency dependence of k($\tilde{\nu}$).

1. Doppler broadening -- result of the relative motion of the absorbers and the observer.
2. Natural broadening -- associated with the radiative lifetime through the Heisenberg uncertainty principle.
3. Lorentz broadening -- result of collision with nonabsorbing molecules.

These phenomena are independent of each other, and may be composed by convolution. The result is Voigt's distribution (Mitchell and Zemansky, 1934).

Given the broadening parameter, which relates natural, Lorentz, and Doppler broadening, one may calculate the shape of a spectral line. Experimentally determined values of the broadening parameter, as a function of temperature and pressure, are available in the literature (Nadler and Kaskan, 1970).

3.3 Distribution Laws

It has been stated that the integral of the absorption coefficient over a spectral line is proportional to the number of absorbers resident in the lower quantum state corresponding to that transition. Assumption of thermal equilibrium allows the use of the Boltzmann law to determine the absolute number of molecules of a species from knowledge of the number of that species in a known quantum state i. This relation may be written as:

$$\frac{N_i}{N} = \frac{1}{F(T)}\, g_i \left[\exp\left(\frac{-E_i}{kT}\right)\right] \qquad (3.6)$$

where g_i is the statistical weight of state i, E_i is the energy of state i, k is the Boltzmann constant, and F(T) is determined by expressing N as the sum of N:

$$N = \sum_i N_i = \frac{N}{F(T)} \sum_i g_i [\exp(\frac{-E_i}{kT})] \tag{3.7}$$

Therefore:

$$F(T) = \sum_i g_i [\exp(\frac{-E_i}{kT})] \tag{3.8}$$

The population distribution in rotational states of a given vibrational state is given by equation (3.6), where the rotational energy is represented as E_i. The degeneracy of the state is equal to (2J" + 1). Rotational term values corresponding to rotational energy are denoted as F(J") (cm^{-1}):

$$F(J") = \frac{E_{J"}}{hc} \tag{3.9}$$

where J" is the rotational quantum number of the absorbing state. The term value is dependent on the rotational quantum number of the lower energy state and the rotational constant of the molecule. The normalization factor, F(T), is, in this case, the rotational partition function, Q_{rot}.

The population distribution in vibrational states is also given by equation (3.6). In this case, E_i is the vibrational energy of absorbing state v". The degeneracy in all vibrational states is 1. The relationship between the energy level and the vibrational term value is:

$$G(v") = \frac{E_{v"}}{hc} \tag{3.10}$$

The vibrational term value is dependent on the vibrational quantum number of the absorbing state, v", and the vibrational constant for the molecule. In this case, the normalization factor is known as the vibrational partition function, Q_{vib}.

Combination of the above relations yields an equation enabling one to calculate N, the absolute number of molecules in the ground electronic state, as the product of a set of spectroscopic constants and an experimentally derived quantity, K, the integrated absorption.

3.4 Definitions and Development of Basic Equation

It was stated in section 2.2 that, when parallel light from a source emitting continuous radiation is sent through an absorbing medium, the intensity of transmitted light, $I(\tilde{\nu})$, will have a frequency distribution according to the equation:

$$I(\tilde{\nu}) = I_0(\tilde{\nu}) \exp [-k(\tilde{\nu})\ell] \qquad (3.3)$$

for sufficiently weak $I_0(\tilde{\nu})$.

The following presentation of theory will develop the phenomenological relationships between spectroscopic constants and the experimentally determined absorption coefficient. Rigorous and precise development of theory may be found in various fundamental texts on molecular spectroscopy (e.g., Mitchell and Zemansky, 1934; Penner, 1959; Herzberg, 1971; Steinfeld, 1974).

This development requires definition of the so-called Einstein probability coefficients:

$B_{12}I_\nu$ = probability (per second) that the atom or molecule in state 1, exposed to isotropic radiation of intensity I_ν and frequency between ν and $\nu + d\nu$, will absorb a quantum $h\nu$ and pass to state 2.

A_{21} = probability (per second) that the atom or molecule in state 2 will spontaneously emit, in a random direction, a quantum $h\nu$ and pass to state 1.

$B_{21}I_\nu$ = probability (per second) that the atom or molecule will undergo the transition from 2 → 1 when it is exposed to isotropic radiation of intensity I_ν and frequency between ν and $\nu + d\nu$, thereby emitting a quantum in the same direction as the stimulating quantum.

In the consideration of two levels coupled by an allowed transition, it is seen that the rate of transitions from the lower level to the upper level is equal to $N_1B_{12}I_\nu$, and that the rate of transitions from the upper level to the lower level is equal to $N_2(B_{21}I_\nu + A_{21})$. At equilibrium, these two rates are equal to each other. Through Boltzmann's law and Planck's black-body law, it is seen that these conditions must be met (Mitchell and Zemansky, 1934):

$$B_{12} = B_{21}\left(\frac{g_2}{g_1}\right) \tag{3.11}$$

$$A_{21} = \left(\frac{8\pi h\nu^3}{c^3}\right)\left(\frac{g_2}{g_1}\right)B_{21} \tag{3.12}$$

In this treatment, the B coefficients are defined in terms of radiation intensity, I_ν, and have units of time/mass. In the original

development by Einstein, B coefficients were defined in terms of spectral density, $\rho(\nu)$, and have units of length/mass. Therefore, $B^I = \left(\frac{1}{c}\right)B^\rho$.

Equation 3.3 was derived from the differential absorption law:

$$- dI(\nu) = I_0(\nu)k(\nu)d\ell \tag{3.13}$$

Equilibration of the rate of energy removal from the light beam to the net rate of the product of the upward transitions and energy per quantum, $h\tilde{\nu}$, leads to:

$$- d[I(\nu)\delta\nu] = N_1 hc\nu B_{12} I(\nu)d\ell - N_2 hc\nu B_{21} I(\nu)d\ell \tag{3.14}$$

where $\Delta\nu$ is the frequency range over which the molecules in levels 1 and 2 can absorb or emit. Molecules undergoing spontaneous emission are neglected, as this emission occurs in all directions.

Assumption of constant $\tilde{\nu}$ over width of line, and rearrangement of equation (3.14), gives:

$$\frac{-1}{I(\tilde{\nu})}\frac{dI(\tilde{\nu})}{d\ell}\delta\tilde{\nu} = h\tilde{\nu}(B_{12}N_1 - B_{21}N_2) = k(\tilde{\nu})\delta(\tilde{\nu}) \tag{3.15}$$

If $N_2 << N_1$, true for $h\tilde{\nu} >> kT$, and $I_0(\tilde{\nu})$ sufficiently small so that equilibrium populations are not significantly perturbed, populations in in N_2 may be neglected. Integration over the absorption line leads to the following equation for B_{12}:

$$B_{12} = \frac{\int_{\text{line}} k(\tilde{\nu})d\tilde{\nu}}{8\pi^2\tilde{\nu}_0^{\,2}e^2}\frac{g_1}{g_2}A_{21} \tag{3.16}$$

Another measure of absorption is the oscillator strength, defined as:

$$f_{12} = \frac{mc^3}{8\pi^2 \tilde{\nu}_0^2 e^2} \frac{g_1}{g_2} A_{21} \tag{3.17}$$

Substitution of B_{12}^{ρ} for A_{21}, and the integrated absorption for B_{12}^{ρ}, leads to:

$$\int_{\text{line}} k(\tilde{\nu}) d\tilde{\nu} = \frac{\pi e^2}{mc^2} N_1 f_{12} \tag{3.5}$$

For purposes of clarity, the oscillator strength will henceforth be referred to as $f_{J''J'}$.

For the OH molecule, the oscillator strength, $f_{J''J'}$, is related to the band oscillator of the rotationless molecule $f_{v''v'}$, by the equation (Anketell and Pery-Thorne, 1967):

$$f_{J''J'} = \left(\frac{f_{v''v'}}{4} \right) \left[\frac{S_{J''J'}}{(2J''+1)} \right] T_{J''J'} \tag{3.18}$$

where $S_{J''J'}$ is the theoretical rotational line strength, $T_{J''J'}$ is the vibration-rotation correction factor (both tabulated in Dieke and Crosswhite, 1962), and J'' is the rotational quantum number of the absorbing state. Although the exact value of $f_{v''v'}$ is under debate, most researchers agree on the approximate value of 9.6×10^{-4} (e.g., Schmidt and Malte, 1976).

The distribution laws give the relationship between the number of absorbers in the particular quantum states and the absolute concentrations in all states. The equation relating N with the absolute concentration N_0 is:

$$N_{J''} = \left[N_0 \frac{(2J''+1)}{Q_{rot} Q_{vib}} \right] \exp \left\{ - \left[F(J) + G(v) \right] \frac{hc}{kT} \right\} \tag{3.19}$$

A description of Q_{rot} and Q_{vib} were given in section 3.3. Exactly, the values of the partition functions are:

$$Q_{rot} = \sum_i g_i \exp \left[\frac{-hcF(J)_i}{kT} \right] \tag{3.20}$$

$$Q_{vib} = \sum_i \exp \left[\frac{-hcG(v)_i}{kT} \right] \tag{3.21}$$

where the index i refers to all the rotational and vibrational levels; and F(J) and G(v) are the rotational and vibrational term values, respectively. The following approximations are commonly made:

$$Q_{rot} = 3.96 \left(\frac{kT}{hcB_e} \right) \tag{3.22}$$

$$Q_{vib} = \left[1 - \exp \left(\frac{-hc\omega_0}{kT} \right)\right] \tag{3.23}$$

where B_e is the rotational constant of a particular electronic state and and ω_0 is the vibrational constant of that state. Spectroscopic constants and other pertinent constants are given in Appendix A. The factor 3.96 arises in Q_{rot} due to lamba- and spin-doubling of the $^2\pi$ electronic of ground state OH (Anketell and Pery-Thorne, 1967). The rotational and vibrational term values of the OH molecule are taken from Dieke and Crosswhite (1962).

Combination of equations (3.16) through (3.23) results in the following equation relating the integrated absorption to the number density in the ground state:

$$\int_{\text{line}} k(\tilde{\nu})d\tilde{\nu} = \frac{\pi e^2}{mc^2} \frac{f_{v''v'}}{4} S_{J''J'} T_{J''J''} \frac{N_0}{Q_{rot} Q_{vib}}$$

$$\exp\left\{ \frac{-[F(J'') + G(v'')]hc}{kT} \right\} \qquad (3.24)$$

3.5 Voigt Profile

Absorption lines are not infinitely narrow, but exhibit depth due to broadening. The broadening factors which affect the absorption coefficient have been discussed in section 3.2. The relations for these factors are (Mitchell and Zemansky, 1934):

1. Doppler broadening:

$$\Delta\nu_D = 2\nu_0 \sqrt{\frac{2kT}{Mc}} \sqrt{\ln 2} \qquad (3.25)$$

2. Natural broadening:

$$\Delta\nu_N = \frac{A_{21}}{2\pi} \qquad (3.26)$$

3. Lorentz broadening:

$$\Delta\nu_L = \frac{Z}{2\pi} \qquad (3.27)$$

where M is the molecular mass and Z is the collisional cross-section.

Of the above, only $\Delta\nu_L$ is not available by *a priori* calculation. However, it may be calculated by its relation to the other factors through the broadening parameter, a, which has been correlated empirically as a function of temperature and pressure. Often, if a researcher has an adequate optical system, the broadening parameter is determined experimentally from the "curve of growth" technique (Penner, 1959).

In the case of broadening effects due to the aforementioned factors, the absorption coefficient is given by Mitchell and Zemansky (1934):

$$\int_{\text{line}} k(\tilde{\nu})d\tilde{\nu} = k_0 \frac{a}{\pi} \int_{-\infty}^{\infty} \frac{\exp(-y^2)dy}{a^2 + (\omega-y)^2} \tag{3.28}$$

where

$$a = \frac{\Delta\nu_N + \Delta\nu_L}{\Delta\nu_D} \sqrt{\ln 2} \simeq 450 \sqrt{\frac{P}{T}}$$

$$\omega = \frac{(\nu-\nu_0)2\sqrt{\ln 2}}{\Delta\nu_D}$$

$$y = \frac{2\delta\sqrt{\ln 2}}{\Delta\nu_D}$$

$$k_0 = \frac{2}{\Delta\nu_D} \sqrt{\frac{\ln 2}{\pi}} \frac{\pi e^2}{mc^2} N_{J''} f_{J''J'}$$

where δ is a variable distance from $(\nu-\nu_0)$. There are a number of recent publications concerning numerical approximation of the Voigt profile, applicable to hand-held calculators (Sulzmann, 1983) or microcomputers (Whiting, 1968; Drayson, 1976).

3.6 Slit Function Effects

As a spectral line is observed by a spectrometer, its shape is distorted by the instrument. The poorer the resolution of the instrument, the greater the distortion. In this case:

$$I(\tilde{\nu}) = I_0(\tilde{\nu}) \exp[-k(\tilde{\nu})\ell d\tilde{\nu}] = \frac{\int_{\sigma} \sigma(\nu,x) \exp[-k(x)\ell]dx}{\int_{\sigma} \sigma(\nu,x)dx} \tag{3.29}$$

where $\sigma(\tilde{\nu},x)$ is the slit function at frequency $\tilde{\nu}$, and represents the intensity of radiation as a function of frequency transmitted by the spectrometer when the latter is on $\tilde{\nu}$.

The slit function may be calculated and applied to the observed absorption line shape as a correction (Hardy and Young, 1949; Kowstowski and Bass, 1956). It is also possible to empirically determine the slit function by using a line source, e.g., a mercury lamp. Often, an effective spectral line shape is assumed; most commonly, a triangular slit function is used.

3.7 Application to System

The above discussion entails the correct means to determine spectral line shapes measured in absorption. Integration of the resultant absorption coefficient, corrected to fit the Voigt profile and for slit width distortion, will avail the calculation of absolute concentration of the absorbing species and spectroscopic temperatures if thermal equilibrium holds.

The limitations of our optical system, however, deem another approach. The greatest spectral resolution possible with the 0.35-m monochromator with the diffraction grating in use is approximately 0.3 Å. An adequate signal-to-noise ratio requires the slits open to about 50 μm for the opposed-jet optical system, resulting in resolution of about 1.3 Å (14.7 cm^{-1}).

To simplify the data reduction scheme, the following assumptions are made:

1. For an optically thin medium, i.e., short optical path length and low absorber density, which results in peak absorption of 15 percent or less, the "weak line" approximation may be made by:

$$\ell \int_{\text{line}} k(\tilde{\nu})d\tilde{\nu} = \int_{\text{line}} \left[\frac{I_0(\tilde{\nu})-I(\tilde{\nu})}{I_0(\tilde{\nu})} \right] d\tilde{\nu} \qquad (3.30)$$

2. When the exit and entrance slits of the monochromator are equal, the slit function may be assumed to be triangular. Thus, the observed spectral line will take a triangular shape.
3. If the spectral slit width is large compared to the actual width of the absorption line, it may be assumed that, at line center, the absorption line lies entirely within the spectral slit width.

When these conditions hold, the following equation relating peak absorption to integrated absorption may be derived (Bleekrode and Nieuwpoort, 1965; Jessen and Gaydon, 1969; Bulewicz et al., 1970):

$$\left[\frac{I_0(\tilde{\nu})-I(\tilde{\nu})}{I_0(\tilde{\nu})} \right]_{\text{peak}} \simeq \frac{\ell}{\Delta\tilde{\nu}} \int_{\text{line}} k(\tilde{\nu})d\tilde{\nu} \qquad (3.31)$$

where $\Delta\tilde{\nu}$ is the spectral slit width, approximately 14.7 cm^{-1} in this study.

Equation (3.24) is used to determine the rotational temperature at a plane in the flame. In an isothermal region (the optical path length), where the absolute number of OH is constant, equation (3.24) may be rearranged to give:

$$\ln \left[\frac{\int_{\text{line}} k(\tilde{\nu})d\tilde{\nu}}{S_{J''J'}T_{J''J'}} \right] = - \left[\frac{F(J'')+G(v'')hc}{kT} \right] \qquad (3.32)$$

A plot of:

$$\ln\left\{\frac{\left[\frac{I_0(\tilde{\nu})-I(\tilde{\nu})}{I_0(\tilde{\nu})}\right]_{peak}}{S_{J''J'}T_{J''J'}}\right\} \text{ vs. } \frac{[F(J'')+G(v'')]hc}{k}$$

results in a straight line if thermal equilibrium holds. The slope of the line is equal to $\frac{-1}{T}$. The temperature calculated in this way is the rotational temperature.

CHAPTER 4

EXPERIMENTAL

4.1 Flame Systems

The laminar, opposed-jet diffusion flame, associated gas flow and analysis systems (Figures 4.1 and 4.2), and operating procedures have been described in detail elsewhere (Hahn and Wendt, 1981; Corley, 1984). A brief description of the system is given here. Burner diameter is 10 cm. Burner spacing of 3.20 cm has been shown to provide steady flames. Stable species profiles are determined by extractive sampling, then gas analysis. Kinetic temperatures are measured with R-type thermocouples (Pt vs. Pt/13%Rh), and corrected for radiation.

The diffusion flame is quite steady. One-dimensionality has been shown to exist over at least 60 percent of the optical path length across the burners. The steadiness and homogeneity of the path length are significant since absorption is a line-of-sight measurement and flickering will lead to unsteady, Schlieren-type deflections of the beam.

The flame studied consisted of the following gas flows:

1. Top burner (gas velocity = 7.78 cm/sec):

CO	6.99 l/min	18.46%
H_2	2.94 l/min	7.78%
He	27.92 l/min	73.76%

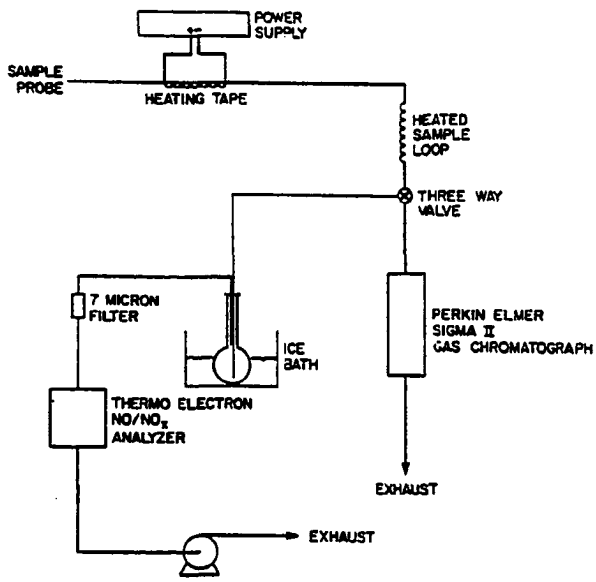

Figure 4.1 Schematic of analysis train.

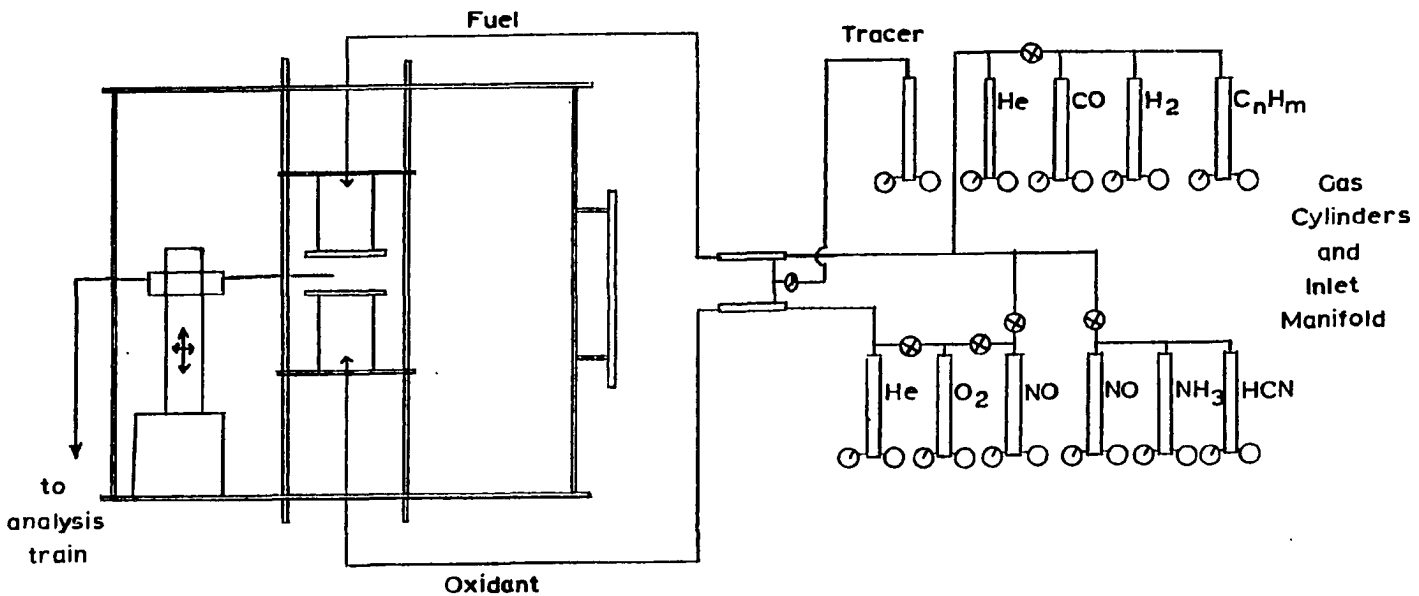

Figure 4.2 Combustor and feed lines.

2. Bottom burner (gas velocity = 4.96 cm/sec):

O_2	10.40 l/min	43.14%
He	13.71 l/min	56.85%

A premixed flame (Figure 4.3) was originally intended to serve as a calibration source. The 18-cm long burner cylinder was made of stainless steel and filled with glass beads to randomize gas flow. The flame was stabilized on a stainless steel grid sitting on a porous metal disc. The burner diameter was 5.5 cm, which was also the optical path length.

The premixed burner was placed inside a quartz chimney 65 cm high and 18 cm in diameter. The chimney was topped with an asbestos pad with a 3-cm hole in its center. Two 0.5-cm holes were formed in the chimney opposite each other to provide optical access. The burner was secured to a jack stand so that optical measurements could be taken at any height from the burner surface to 2 cm above the burner.

An R-type thermocouple with a 10-mil bead provided temperatures at the optical plane. The temperatures were measured close to the center of the burner.

A near stoichiometric methane/air mixture was provided to the burner at a rate of 35 cm/sec. The methane flowed through a gas regulator and a rotameter at 4.79 l/min. The air was supplied from a compressor in the building through a 1/2-in. line. The amount of air required precluded use of any regulation except for the valve at the end of the line. Gas flows were measured by a wet-test flowmeter at the beginning and end of each run. Purge helium provided a semi-inert

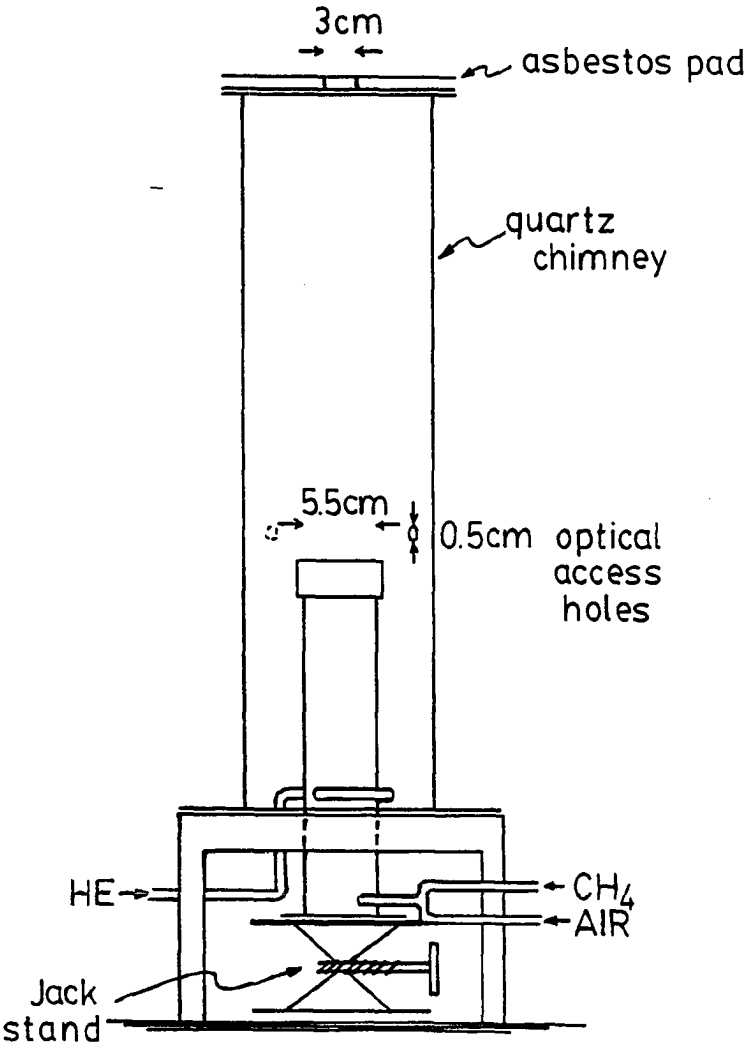

Figure 4.3 Premixed flame for optical studies.

atmosphere; no extraordinary measures were taken to ensure an airtight system.

4.2 Optical System

A schematic of the final design phase of the opposed-jet optical system is shown in Figure 4.4. Light from the arc lamp, collected and focused by a condensor assembly on the lamp housing, was chopped by a mechanical chopper and split by a fused silica flat. All optics must be of ultraviolet grade. Approximately 5 percent of the incident light on the flat was reflected and sent off at an angle to a silicon photodetector, which provided timing signals and monitored changes in beam intensity from the arc lamp. The remainder of the light was directed vertically by a mirror to another mirror. The second mirror reflected the beam horizontally through the combustion regions of the flame, where it was received by a light baffle/optical fiber bundle system (Figure 4.5). The mirror/baffle/bundle system was secured on an aluminum mount, attached to a micromanipulating device. This allowed a vertical scan of the flame.

The optical system for the premixed flame was similar, except that light transmitted through the beam splitter went directly through the flame region to the light baffle.

The attenuated beam was transmitted through the optical fibers, where it exited and was focused on to the entrance slit of a scanning monochromator. The intensity of diffracted radiation was detected by a photomultiplier tube contained in a radio frequency-shielded, light-shielded housing (Pacific Instruments, 3150).

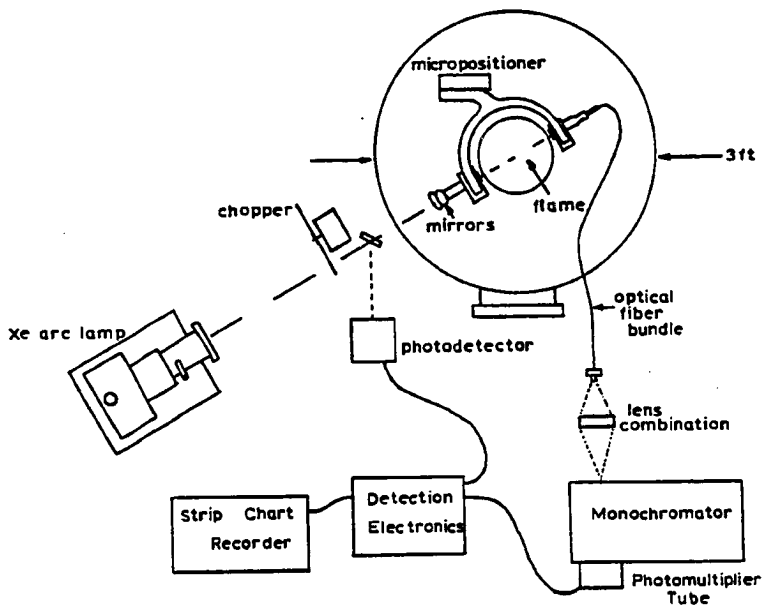

Figure 4.4 Final design phase of opposed-jet optical system.

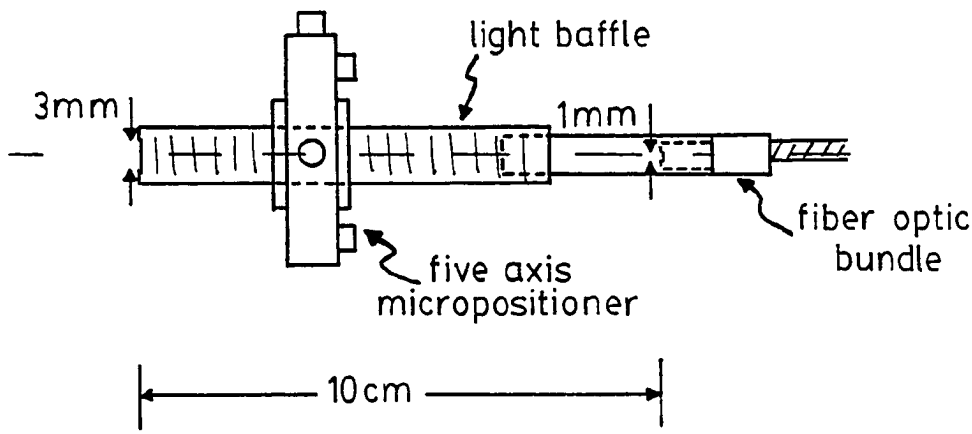

Figure 4.5 Light baffle/fiber optic system.

The output of the photomultiplier tube (pmt) was amplified and sent through the detection electronics, where boxcar integration and analog averaging were done on signals from both the pmt and silicon detector. A ratiometer provided voltage representing I/I_0. This voltage was sent to an analog recorder, which provided a record of absorption vs. wavelength.

Each of the components in the optical system, and any associated operating procedures, is now discussed in detail.

4.2.1 Arc Lamp Source

A 75 W, xenon arc lamp source (Oriel, 6301) with condensing lens assembly (Oriel, 6304, UV grade) provides a stable (less than 1 percent rms ripple) output of continuous radiation in the ultraviolet region. The intensity of radiation smoothly increases with increasing wavelength in the ultraviolet, but may be considered constant over the width of an absorption line.

The arc lamp (Osram, XB075W/2) is a low power source compared to other sources typically used in absorption experiments discussed in the flame literature. This source has the following advantages over larger lamps:

1. The lamp is more stable, exhibiting less ripple and long-term drift.
2. The arc lamp source (lamp, power supply) is much less expensive than larger sources.
3. The arc itself is small (effective arc is 0.25x0.5 mm) and is actually brighter (400 CD/mm^2) than larger sources typically

used. This is a great advantage considering the sample cross-section (approximately 0.8 mm^2) is desired to be small. In effect, the use of larger sources would waste light.

The lamp exhibits maximum stability when operated between 5.0 and 5.2 amps. Lamp ignition requires an extremely high (20-30 K) voltage; safety precautions indicated in the manual should be adhered to.

It was believed that the igniting voltage pulse train damaged op-amps in the near vicinity of the lamp. For this reason, ignition capacitance was decreased, which shortened the ignition time. Also, supply voltage to the power supply was changed to 220 V, which allowed the power supply an isolated wall outlet of its own. As a precaution, any sensitive electronic devices, especially those containing op-amps, were turned off during ignition.

The lamp was susceptible to variations in temperature, resulting in ripple or arc wander; for this reason, convective cooling was provided in the lamp housing. It was observed that, after about 3 hours of operation, arc wander increased; for this reason, it is advised to plan runs of under 3 hours.

4.2.2 Mechanical Chopper

The chopping apparatus consisted of a 20-aperture, chopping blade (Princeton Applied Research, 2517-0341) drived by a 0.1-hp, A.C./D.C. motor (Grainger, 2M037) regulated by an adjustable electronic speed control (Grainger, 4X796). The motor produced considerable electronic noise; therefore, it was enclosed in an aluminum box.

The chopping frequency was predetermined as 200 hz. This frequency was chosen because it provided adequate averaging (average rate = 80 samples/0.4 sec), and would be within "safe" operating limits of the chopper and electronics. Detection electronics were designed on this premise. Optimal chopping frequency lies within an area with a lower limit of period equal to 5 msec and upper limit of period equal to 7 msec. In the course of an experiment, the optimum was found by observing the gating signal (during which integration of signal occurs) and waveforms from the pmt and silicon photodetector simultaneously on a dual-trace oscilloscope (Tektronix, 453A). Minimum noise was accomplished with the gating signal lying entirely within the waveform from the photodetector, and centered as nearly as possible to the center of the waveform from the pmt.

Small variations in chopping frequency presented problems. This proved to be a limiting factor in chopping speed. This could be resolved by the use of a synchronous motor. A change in height of the baseline was symptomatic of this problem.

4.2.3 Beam Splitter

All lenses exhibit a certain amount of non-transmissivity, dependent on the angle of incidence and index refraction of the lens. This was used to an advantage in this application. A fused silica flat (Rolyn Optics, 55.4150) reflected about 5 percent of incident light in the wavelength region of interest, thereby accomplishing the same thing a much more costly beam splitter does.

4.2.4 Silicon Photodetector

An ultraviolet-enhanced, photoconductive, silicon device (EG&G, HUV 1000B) provided the means of measuring unattenuated (no absorption) radiation intensity, and also waveforms for the production of gating signals.

The photodetector collected chopped light reflected off the quartz flat. External, adjustable offset and amplification were provided. The optimal combination of these adjustments with the adjustment of chopping frequency resulted in an optimal signal-to-noise ratio.

The gated integrators in use operate optimally when the input voltage is approximately 1 volt. A shape close to a square wave will provide the best results; this may be achieved by focusing the beam down to a point much smaller than the chopper aperture.

4.2.5 Mirrors

The mirrors used were ultraviolet-quality, aluminum-surfaced (Newport Corp., 10D10AL.2), and were mounted on either five-axis micropositioners (Newport Corp., LP-1-05B) or mirror mounts (Newport Corp., MM-1). The first mirror reflected a horizontal beam 90 degrees to vertical. The second mirror, mounted on a micropositioner mounted on a yoke apparatus attached to the micromanipulator, reflected the vertical beam 90 degrees to horizontal, across the flame on to a baffling device.

4.2.6 Light Baffle

After the light passed through the flame, it entered the machined aluminum light baffle. The opening of the baffle was 3 mm. The length of the baffle was 10.0 cm, and painted black on the inside to

absorb light. The ferrule of the entrance portion of the fiber bundle was fixed to an extension of the light baffle. This arrangement defined the light area incident on the fibers, and served to minimize stray light.

The diameter of the beam of light entering the flame decreased from about 25 mm at the lamp to 4 mm at the entrance of the light baffle, over a distance of about 1800 mm. This results in an average beam diameter of about 3.4 mm through the flame. However, most of the intensity of the light beam was concentrated in the image of the arc, which made up only a fraction of the area of the light beam. For this reason, spatial resolution was not calculable *a priori*, but was deduced from differences in measured absorption at various heights in the flame.

The baffle/fiber bundle ferrule was screwed into a five-axis positioner, which provided fine positioning. The positioner was mounted on to a yoke apparatus, which, in turn, was connected to a micromanipulating device. The aim of this was to make the optical system as monolithic as possible, thus minimizing the effect of any physical perturbations.

4.2.7 Optical Fiber Bundle

The fiber bundle (Maxlight) was utilized to transfer light to and from inaccessible regions of the combustion/optical system. The stainless steel-sheathed bundle was 1 mm inner diameter, with 0.2-mm diameter, fused silica fibers. Although the attenuation of light is rather high at the operating wavelength (approximately 40 percent at

300 nm), it was believed that the advantage, i.e., no need to maintain precarious optical alignment, outweighed this factor.

The fiber bundle was circular at the entrance and arranged in a rectangle (0.2x4.3 mm) at the exit. The purpose of this was to increase the light coupling efficiency between fibers and monochromator, which has a rectangular slit. The exit end of the bundle was mounted on a mirror mount, which allowed fine pitch and yaw adjustment.

4.2.8 Optical Fiber Bundle/Monochromator Coupling Optics

Light exits the fibers at a 15-degree half-angle (F number = 2). The monochromator has collection optics with F number of 6.8. If the light output from the fiber was a point source, the solution of how to couple the fiber output to monochromator input would be trivial. However, the output of the fiber bundle is a collection of point sources; this complicated things considerably. This problem was solved empirically.

A number of lenses of varying focal lengths were borrowed. Various permutations of different lens combinations and distances between objects and images were tried, and the arrangement which yielded maximum light output was chosen. This optical arrangement is shown in Figure 4.6.

If the lenses were achromatic (they were not), the focal point of all wavelengths would be the same. It should be noted that the focal point as determined by the human eye may not be the focal point of ultraviolet wavelengths of interest in this study that the eye is not sensitive to.

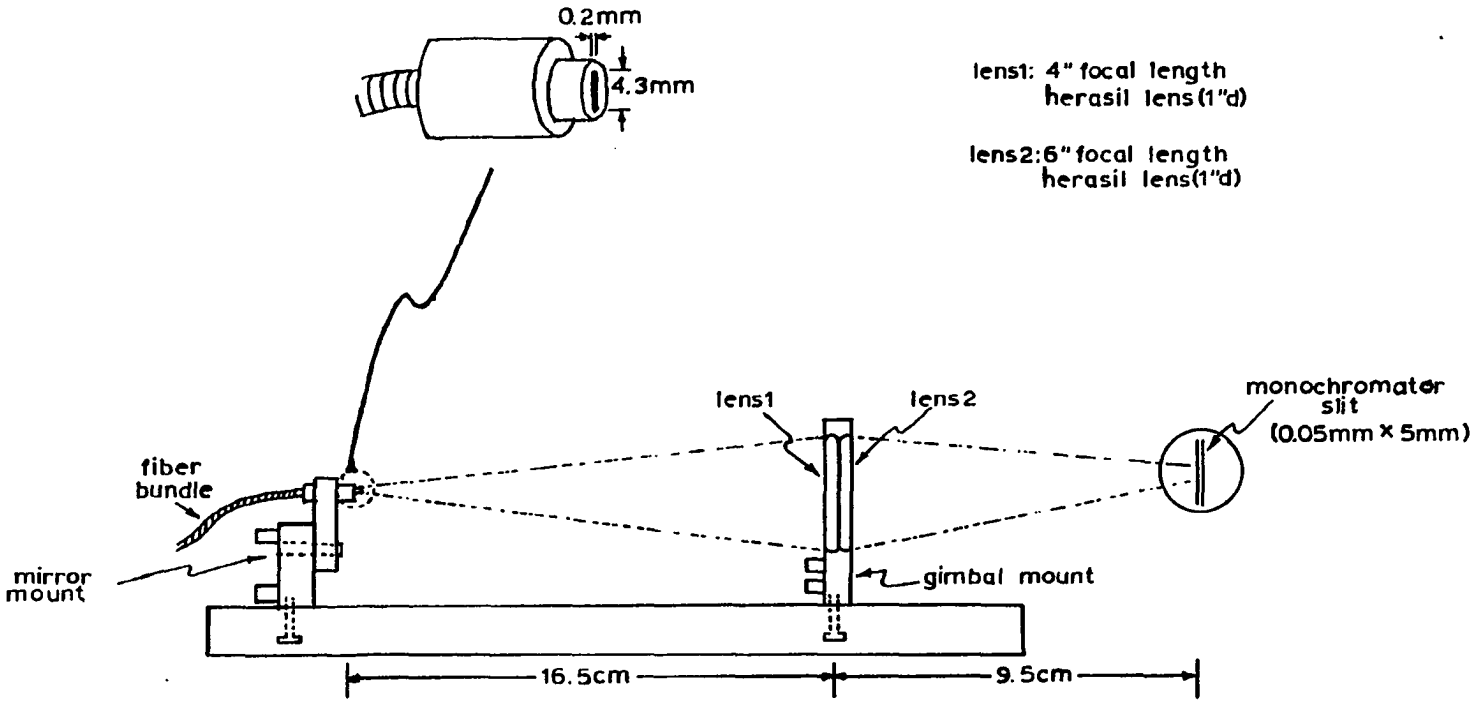

Figure 4.6 Optical fiber/monochromator coupling system.

4.2.9 Monochromator

The instrument (GCA-McPherson, EUE-700) was a scanning, single-pass, Czerny-Turner type. The F number of the collection optics was 6.8. Spectral half-width with 5-μm entrance and exit slits was 0.3 Å. The grating had 1180 lines/mm, and was blazed at 2500 Å. The efficiency of the monochromator at 3000 Å was about 50 percent.

The slit width of the monochromator which afforded the best combination of resolution and signal-to-noise ratio was determined as 35 μm for the premixed flame and 50 μm for the opposed-jet flame. This resulted in respective spectral half-widths of 0.8 and 1.3 Å, which allowed resolution in the strongly absorbing $Q_1(2)$, $Q_1(3)$, $Q_1(4)$, $Q_1(5)$, and $Q_1(6)$ rotational lines. The scan speed of the monochromator was set at the slowest speed (0.05 Å/sec). The monochromator was wavelength-calibrated, and its spectral half-width determined by use of a mercury pen lamp (BHK Inc., 98-0010-01). This lamp put out three Hg emission lines of known intensity in the region of interest.

4.2.10 Photomultiplier Tube
and Power Supply

The photomultiplier tube (pmt) is a 1-1/8 in., side-on type (Hamamatsu, R928). The spectral response range was 185-920 nm, with peak response at 400 nm. The anode sensitivity was 6.8×10^5 A/W. The gain was 1.0×10^7. Typical dark current was 10 na. The equivalent noise input (ENI), i.e., the spectral radiation required to provide a signal-to-noise ratio equal to 1 when only noise inherent in the pmt is present, was approximately 10^{-17} W.

The tube was chosen because of its high quantum efficiency in the region of 300 nm and its low ENI. Preliminary calculations showed light reaching the pmt would be on the order of 10^{-13} W. It was assumed that the pmt has a linear response to light in the region of 310 nm.

The power supply (Pacific Instruments, 204) was a highly regulated, high-voltage power supply. Low ripple and noise are critical in this application.

The pmt was rated at a maximum of 1250 volts. It was recommended that the operating voltage be on the order of 200 volts less. In fact, in the course of experimentation, the optimum operating voltage was found to be between 650 and 800 volts.

4.3 Detection Electronics System

The detection system, as was stated earlier, utilized boxcar integration and analog averaging. An outline of the detection scheme is given in Figure 4.7. A detailed schematic of the circuit design is given in Figure 4.8. A layout of the main circuit board is given in Figure 4.9. The system was a combination of home-built circuits and off-the-shelf, plug-in modules. Schematics and calibration procedures for the modules were provided by the manufacturer and are present in the laboratory.

As is seen from the outline, signals from the pmt and silicon photodetector were amplified (Burr-Brown, INA101AM) and sent to gated integrator modules (Evans Associates, 4130). The integrators received gating signals of 1 msec duration from a programmable, time-delay module (Evans Associates, 4141-3). Integration of signal proceeded

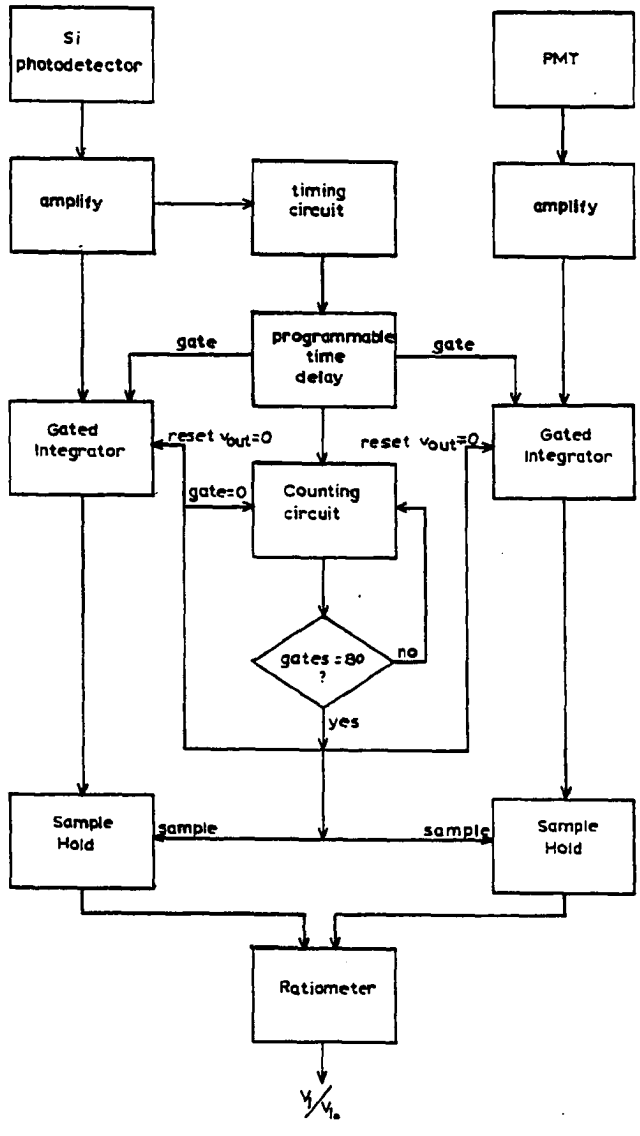

Figure 4.7 Outline of detection electronics.

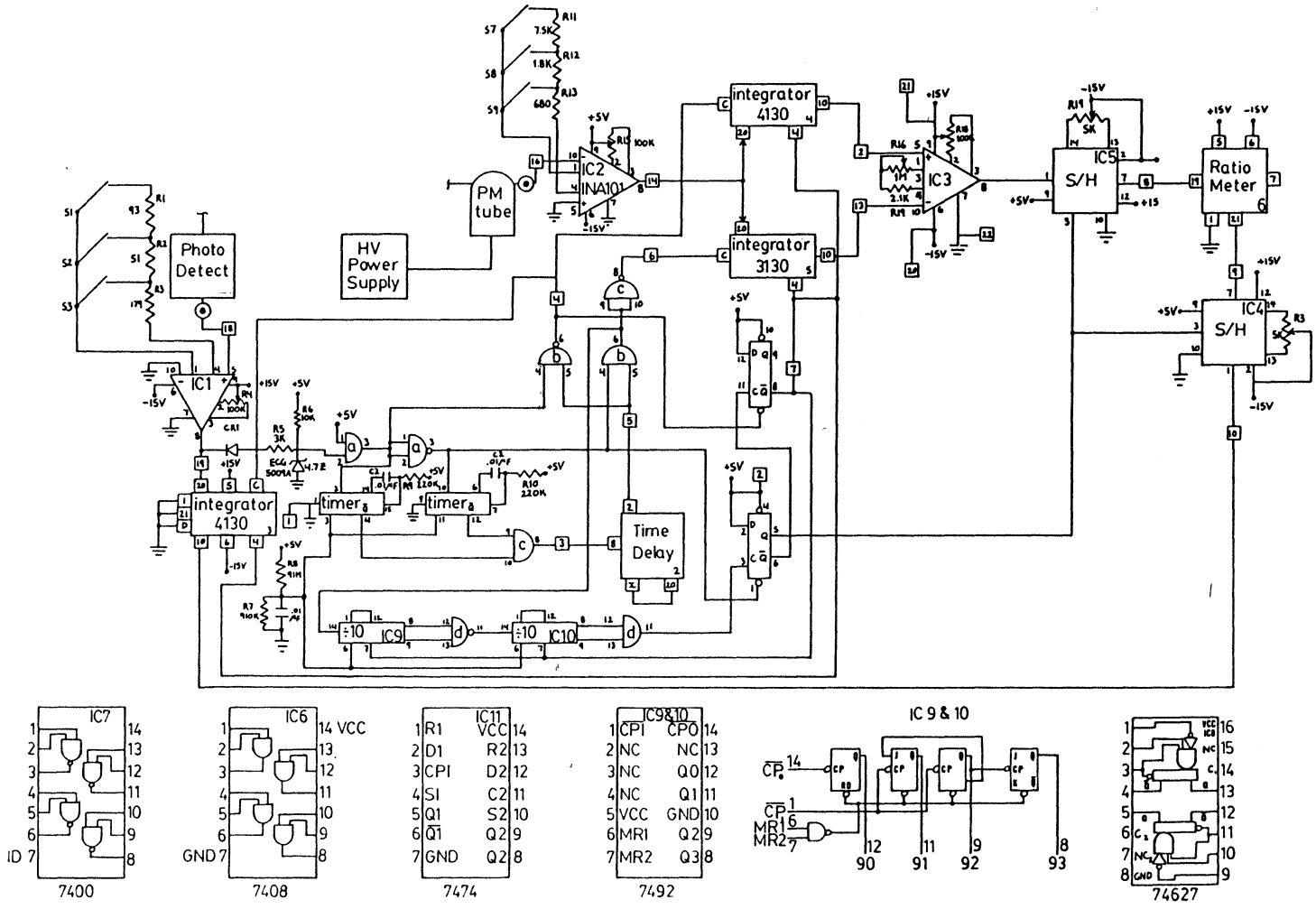

Figure 4.8 Schematic of circuit design.

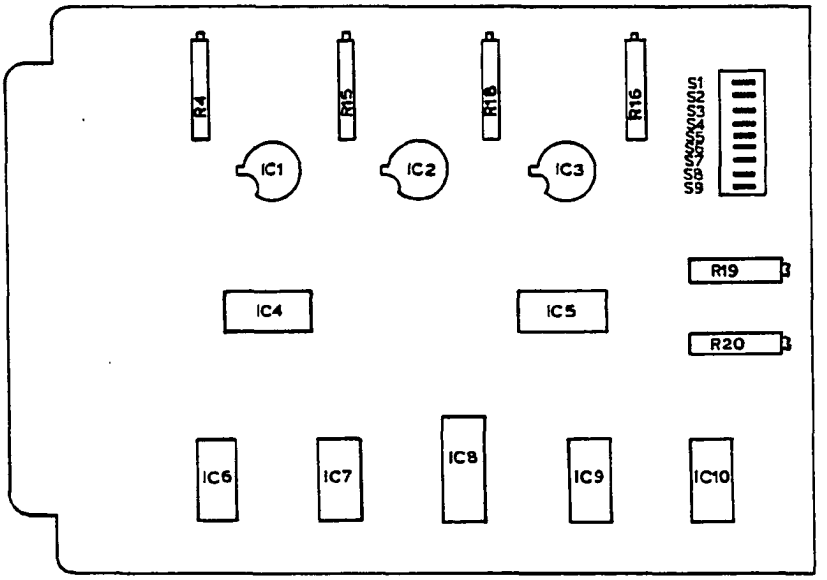

Figure 4.9 Layout of main circuit board.

during open-gate intervals, i.e., when the integrator was receiving a gating signal. During closed-gate intervals, the integral (output of the integrator) was held constant. Utilizing external reset, the module was used in boxcar mode, whereby the integrated voltages were continuously added. In effect, the output of the integrator was the average of the integrated signals.

The gating signals were generated from the programmable, time-delay module. The module generated a time-delayed pulse following a trigger pulse applied to the time-delay module. The width of the time-delayed pulse was externally adjustable from 0-1.5 msec; the length of the delay was fixed. The width of the pulse was limited by the chopping frequency. Integration of as much of the signal as possible was desired. A 1 msec width was found to be about optimal at 200 hz.

The triggering pulse to the time-delay module arose from the positive-going waveform of the output of the amplified signal from the photodetector. The delayed trigger pulse was applied to the module after the signal passed +0.5 volts. Obviously, the waveform must be less than +0.5 volts at its minimum, and more than +0.5 volts at its maximum. A square wave was desired to reduce the effects of jitter.

The offset and amplification of the photodetector signal determined the placing of the gating signal. Offset resulting in a more positive signal had the effect of the waveform attaining +0.5 volts sooner, resulting in a relatively early gating signal. A more negative signal had the opposite effect. In this way, the gate sent to the integrator which integrates the pmt signal was placed at the point which optimized the ultimate signal. The gate sent to the photodetector

integrator must lie safely within the waveform from the photodetector. Typically shaped waveforms are shown in Figure 4.10. It is seen that the relative placement of the gate within the waveform from the photodetector is not critical, as the voltage was constant at the minimum and maximum for a long time relative to the duration of the gates.

A circuit counted the number of gates generated. After 80 gates, a signal was sent to sample/hold circuits to sample the output voltage of the integrators during a closed-gate period. The circuit held that voltage for the next 80 gates. The output voltage from the sample/hold circuit represented the average of 80 samples taken by the integrators over a 0.4-sec period (for 200 hz chopping frequency).

A reset, returning the output voltage of the gated integrators to 0 volts, was actuated immediately after the sample/hold circuit opened. The integrators resumed their integration and summation, and the cycle started again.

The output of the two sample/hold circuits, which represented the unattenuated intensity of light, I_0 (from the photodetector), and the attenuated intensity, I (from the pmt), were sent to a ratiometer (Evans Associates, 4122). The output from the ratiometer represented I/I_0. This voltage was sent to an analog recorder. Simultaneous scanning of the monochromator over the wavelength corresponding to an absorption line resulted in a hardcopy representation of the frequency-dependent absorption coefficient.

The schematic indicates an extra integrating circuit. The original intention was to subtract D.C. flame emission and electronic noise from the signal of the pmt. The integration was timed to occur

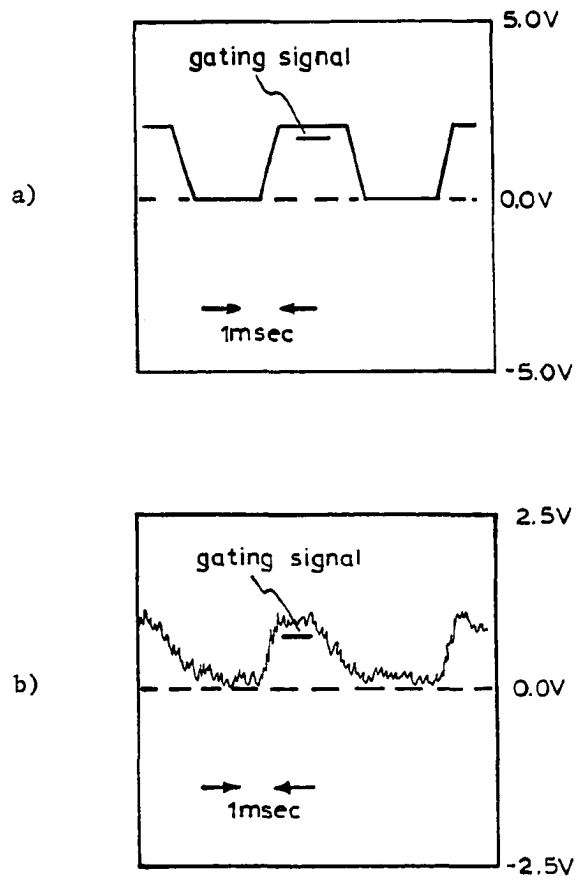

Figure 4.10 Typically shaped waveforms. — a) Photodetector; b) photomultiplier tube.

180 degrees out of phase with the signal representing light absorption. It was quickly discovered that noise levels were much lower when the input to this integrator was grounded, i.e., there was no subtraction of background noise. This was due to nonsymmetry of the waveform from the pmt; minimum and maximum points of the waveform from the pmt were not 180 degrees out of phase with each other. Without the addition of another timing circuit, it was not possible to place gates at the maximum and minimum points simultaneously. However, this is not considered a problem for the following reasons:

1. The flame was steady; no apparent fluctuations were present.
2. Emission, after consideration of attenuation of light due to the optical fiber and light coupling to the monochromator, was very small compared to the intensity of the lamp.
3. Random electronic noise and any short-term fluctuations of the flame were on a much shorter time scale than the integration time; due to their nature, they averaged out over the integration time.
4. Long-term fluctuations averaged out over 80 samples. The signal-to-noise ratio theoretically improved as the square root of the number of samples taken.

4.4 Operating Procedure

Procedures specific to each component were discussed earlier. The experimental procedure is given here. First, the rotational lines to be studied were chosen. Second, satisfactory optical alignment was

achieved. Third, the chopping frequency was set to the optimal speed. Finally, scans of the absorption lines were done.

4.4.1 Choice of Absorption Lines

Dieke and Crosswhite (1962) list the wavelength, analysis, and transition probabilities of all rotational lines in the electronic transition studied. The two most important criteria to be met are: 1) evidence of measurable absorption must be present, and 2) the absorp- should not be affected by absorption of other lines. Lines separated by at least 1.0 Å from other strongly absorbing lines are chosen. The intensity of emission of a line at 3000 K, tabulated by Dieke and Crosswhite, provided an arbitrary means of determining which lines were "strongly" absorbing. Practically, if the intensity of emission of a close (1.0 Å) line was on the order of 10 percent or less of the intensity of emission of the absorption to be studied, it was considered to have negligible effect on the measured absorption of the main line.

Theoretically, one may calculate the rotational quantum number of the most heavily populated quantum states at a given temperature. As derived by Mavrodineanu and Boiteux (1965), the quantum numbers corresponding to the most heavily populated levels of a heteronuclear, diatomic molecule are:

$$J_{max} = \sqrt{\frac{kT}{2hcB}}$$

At 2000 K, $J_{max} = 6$ or 7.

In practice, lines to be studied are determined as follows:

1. A quick scan (0.1 Å/sec) of the wavelengths from 305 nm to 315 nm is done. All major rotational transitions occur within this region.
2. Dominant absorption lines are noted and assigned according to Dieke and Crosswhite (1962).
3. The "isolated line" criteria are applied.
4. Wavelength regions which contain a series of appropriate absorption lines are determined.

Since the population distributions will shift according to temperature, it is recommended to check for any significant differences in step 2 above for different regions of the flame. However, it has been seen that the J" = 2, 3, 4, 5, and 6 levels of the Q branch are suitable throughout the flame. These have line centers at λ = 3080.0, 3081.5, 3083.3, 3085.2, and 3087.3 Å, respectively. Thus, a slow scan from λ = 3078 Å to 3090 Å will include these lines.

4.4.2 Achievement of Optical Alignment

The lamp, chopper, beam splitter, and photodetector were situated upon an optical bench. Their alignment was a simple matter of rotating the beam splitter while observing the amplified voltage output of the photodetector, and fixing the beam splitter where the voltage was a maximum.

It appeared easier to detect the effect of changes in alignment while observing the chopped signal. This was accomplished by attaching

the oscilloscope probes to pin 19 of the main circuit board or pin 20 (D.C. signal input) of the integrator wired to pin 19.

There were three adjustments on the lamp housing which affected the shape and intensity of the light beam. They need only be done once, with periodic checks. On the top of the lamp housing was a knob which afforded vertical and rotational placement of the arc lamp. The correct placement was attained by observing the light output and adjusting for maximum uniformity and amount of visible light. If an image of the arc was present, the knob should be adjusted to place the arc in the center of the beam.

Two adjustments were located on the condensor housing. One (part A) determined the placement of the primary condensing lens. The second (part B) determined the focal length of the light beam, given fixed part A.

These adjustments may not be done independently. They also may not be done visually. The intensity of radiation reaching the pmt must be observed on the oscilloscope by attaching the probe of the scope to pin 14 of the main circuit board. The procedure was as follows:

1. Adjust part B to give the resultant focal point location at the entrance of the light baffle.
2. Adjust part A to result in maximum signal as seen on the oscilloscope.
3. Adjust part B to give maximum signal.
4. Repeat steps 2 and 3 as necessary.

Gross optical alignment of the rest of the system was achieved visually, starting from the front end and proceeding to the back. That is, the first reflecting mirror was adjusted to give as nearly a vertical beam as possible. If the beam was vertical, and if the movement of the micromanipulator was strictly vertical, a complete vertical scan of the flame could be done. If this alignment cannot be done, limited vertical scans or discrete planar measurements, with realignment each time, must be done. Obviously, the former situation was desirable.

The second mirror was adjusted to send the reflected beam horizontally across to the light baffle. This was done by removing the fiber bundle from the baffle, placing a white card close to the exit of the baffle, and adjusting either or both of the five-axis micropositioners (one holds second mirror; the other holds the light baffle) so the beam exited at the center of the baffle.

Once this gross alignment was done, optical alignment of the fiber optic/monochromator coupling was done. Again, this was first done visually, by observing the placement of the image of the output of the fiber bundle on the slit of the monochromator. Figure 4.6 (page 52) serves as a first approximation as to where the various components should be placed.

The probes of the oscilloscope were then attached to the amplified output of the signal from the pmt (pin 14 on the main circuit board or pin 20 on the integrator). Again, use of the chopped signal seemed to make detection of slight changes easier.

While observing the voltage signal from the pmt on the oscilloscope, the entire apparatus was moved by hand. One degree of rotational,

and two degrees of translational, movement must be done. It was assumed that the correct vertical orientation may be accomplished visually.

At some point, gross manual movement of the entire fiber bundle/monochromator coupling apparatus resulted in maximum signal on the oscilloscope. Adequate means of securing the apparatus were done. Actually, if the table is not disturbed, the apparatus is heavy enough to remain in place.

Fine adjustment of the coupling optics was then accomplished by use of the gimbal mount, on which the ferrule of the fiber bundle was attached. The alignment was independent of the rest of the optical system. It was discovered that slight movements, e.g., changing the setting of the scanning motor, affected this alignment. Adjustment of the gimbal mount remedied the slight misalignment.

It was now only necessary to fine tune the alignment of the micropositioners attached to the yoke apparatus. The pmt signal was observed on the oscilloscope and the adjustments on the five-axis positioner holding the fiber bundle were made to give the maximum signal. Usually, the adjustment of all five axes is not necessary. Adjustment of vertical, horizontal, and one of the rotational axes sufficed.

During the course of a run with the opposed-jet configuration, misalignment due to thermal expansion caused partial or complete loss of signal. Also, vertical scanning caused partial losses at times. It was relatively simple to regain alignment by slightly adjusting the mounting screws on the lamp housing and monitoring the signal. This could usually be done by rotating only one of the screws by no more than 1/4 turn in either direction. This became more difficult in the regions

above the flame front, where the light must pass through regions of steep temperature gradients. Deflection of the beam due to Schlieren effects occurs here. However, this was not really a problem, since, at this point in the flame, OH concentrations have been decreased to the point of minimal detection.

The above procedures were developed from experience and followed in experimentation. True appreciation is not possible without a good deal of experience with the system.

4.4.3 Achievement of Optimal Gate Placement

The causes and effects of chopping frequency and gate placement have been discussed previously. The method of achieving the optimal frequency is as follows:

1. All components of the system must be on.
2. Attach channel A probe to pin 19 of the main circuit board.
3. Turn trace control to "A." Waveforms representing the amplified signal from the photodetector should be displayed. It is assumed that optical alignment has already been optimized.
4. Adjust offset and/or amplification to result in waveforms with minimum at approximately 0.2 V and maximum at 1.0-2.0 V.
5. Adjust electronic speed control on chopper to result in waveforms of 6.0±0.5 msec.
6. Attach channel B probe to pin C of any of the integrators.
7. Turn trace control to "A + B chopped." If steps 4 and 5 above have been done correctly, gating signals of 1 msec located at

about the center of the maximum of the waveform will be displayed.

8. If gates are sporadic, or interfering with the waveform from the photodetector, adjust offset to get gate stability.
9. Attach channel A probe to pin 14 (amplified signal from pmt) of the main circuit board.
10. Adjust offset to center gating signal as close as possible to maximum of pmt waveform.
11. Fine tune offset to completely satisfy step 8, while satisfying step 10 as much as possible.

Over the time of an experiment, the chopping frequency may wander outside of safe operating limits (6.0±0.5 msec period). Therefore, the situation as described in step 7 above was monitored throughout the experiment. It may be necessary to periodically adjust the electronic speed control to maintain the correct chopping frequency.

4.4.4 Scan of the Absorption Lines

The wavelength region to be scanned has already been determined. The chart recorder speed was set at 4.0 cm/min. The scan speed on the monochromator was set at 0.05 Å/sec. This corresponded to 0.75 Å/cm on the recorder. The scan was started at 3078 Å. The drivers for the scanning motor and chart motor were engaged simultaneously. The scan was terminated at 3090 Å.

At least two, and usually three, reproducible scans over the wavelength region were done for each placement in the flame. After the set of scans, the yoke apparatus was moved to a new height in the flame.

Measurements at approximately every 0.5 cm were taken in the active combustion region (1.3-1.6 cm below the top flange), and less resolute measurements were made outside this region.

The chopping frequency, gating placement, and unattenuated light intensity were monitored simultaneously on the oscilloscope during the run. Unless absolutely necessary, it was desirable not to make any adjustments during a scan, but between scans.

After the scan, realignment of the fiber/monochromator optics was done simply by adjusting the gimbal knobs. The monochromator was returned to 3078 Å.

It was necessary to know the temperature of the space the absorbed light traversed. For the premixed flame, an R-type thermocouple, with bead of 10 mil, was placed in the horizontal plane of the light beam, slightly removed to the side out of the optical path. The bead was centered as close to the center of the burner as was possible.

It was assumed the laminar, opposed-jet diffusion flame was reproducible to within the limits of the spatial resolution attainable. Thermocouple measurements of the same flame provided temperature profiles in this case.

The above procedures were developed and followed during experimentation with the premixed flame. Perhaps fortuitously, a problem arose during experimentation with the opposed-jet flame -- the photodetector became "disabled." In its place, a signal generator (Hewlett-Packard, 202A) was used. A square wave of frequency 200 hz and amplitude 1.5 V was fed into the electronics instead of the output of the photodetector. This operating procedure had no ill effects on the data;

in fact, it improved the quality of data considerably. The single-beam set-up was acceptable due to the confirmed stability of the light source.

CHAPTER 5

EXPERIMENTAL RESULTS

5.1 Analysis of Data

Typical absorption scans obtained at approximately 1 mm increments in the $CO/H_2/He$ vs. O_2/He diffusion flame are shown in Figure 5.1. These scans were taken with the monochromator slit width set at 50 μm ($\Delta\tilde{\nu}$ = 14.7 cm^{-1}). The $Q_1(2)$ through $Q_1(6)$ transitions are apparent at λ = 3080.0, 3081.5, 3083.3, 3085.2, and 3087.3 Å, along with a large absorption centered at approximately 3090 Å. The large absorption is due to the combined effects of the $Q_1(7)$, $Q_2(2)$, and $Q_2(3)$ transitions, and is a suitable qualitative indicator of the amount of absorption. Each scan is identified by run number relatable to the designation in Appendix B, which contains raw data in terms of percent peak absorption.

Scans taken with 40 μm slits ($\Delta\tilde{\nu}$ = 11.6 cm^{-1}) are shown in Figure 5.2. The scans with different slit widths cannot be taken as equal since the spectral slit width has a linear effect on calculated concentration. Clearly, this resolution, or better, is desirable. However, the optical alignment necessary to be able to narrow the slits to less than 50 μm was extremely difficult to achieve and only one run of this type was done.

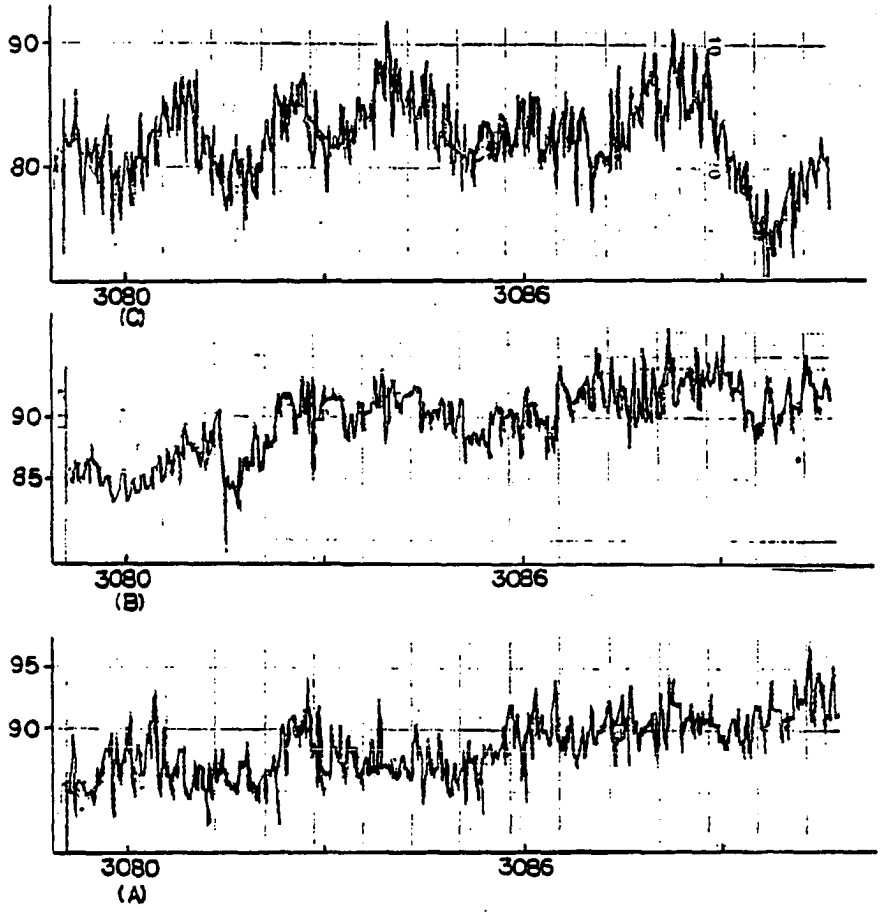

Figure 5.1 Typical absorption scans with 50 μm slit width. -- a) 1.17 cm above bottom flange; b) 1.29 cm above bottom flange (1g); c) 1.41 cm above bottom flange (3b).

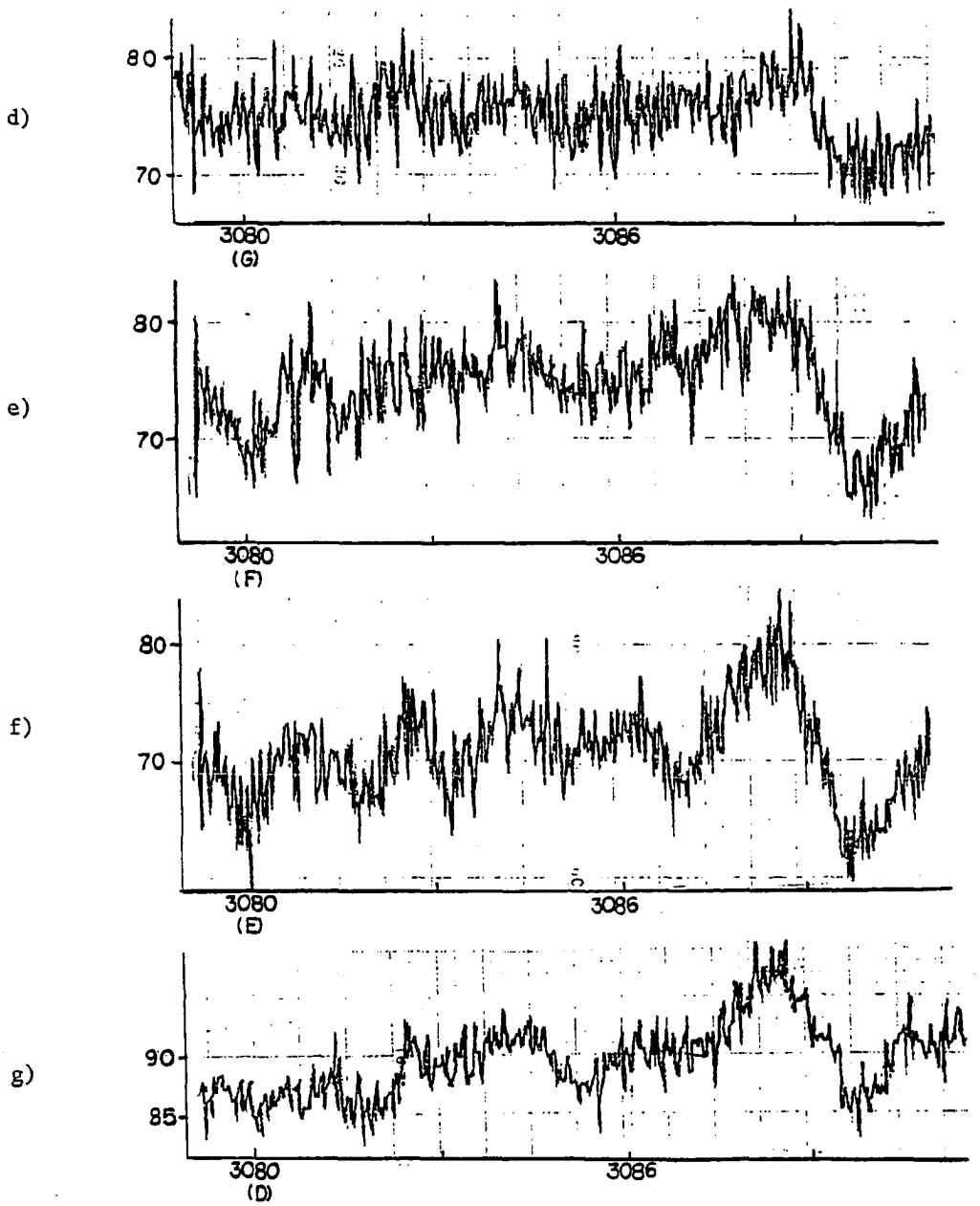

Figure 5.1, Continued. -- d) 1.53 cm above bottom flange (1b); e) 1.72 cm above bottom flange (3e); f) 1.83 cm above bottom flange (3g); g) 1.92 cm above bottom flange (3j).

a)

b)

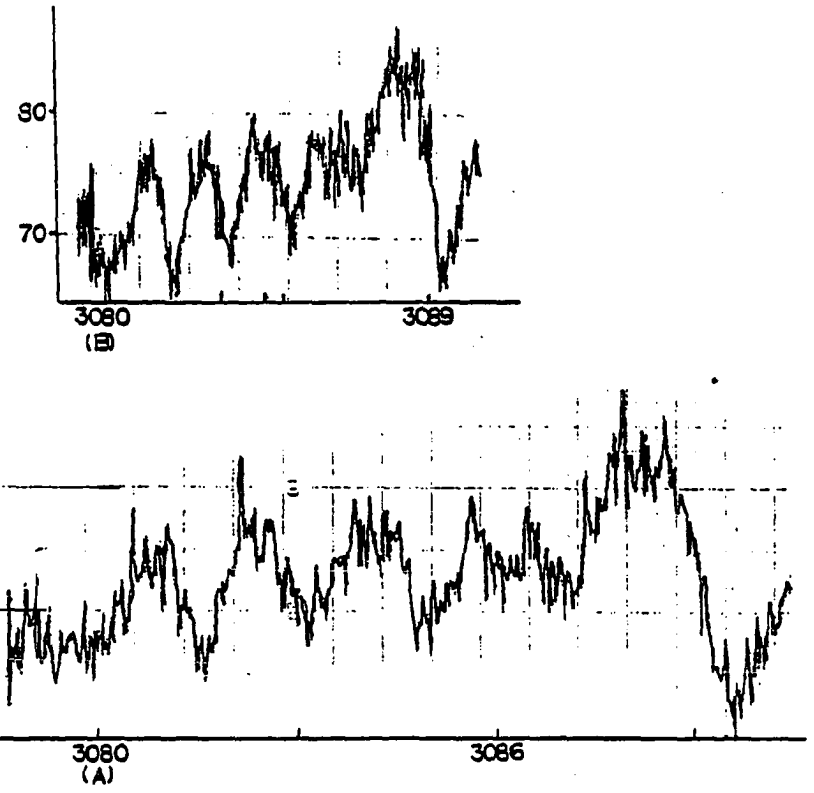

Figure 5.2 Typical absorption scans with 40 μm slit width. -- a) 1.55 cm above bottom flange (4i); b) 1.63 cm above bottom flange (4a).

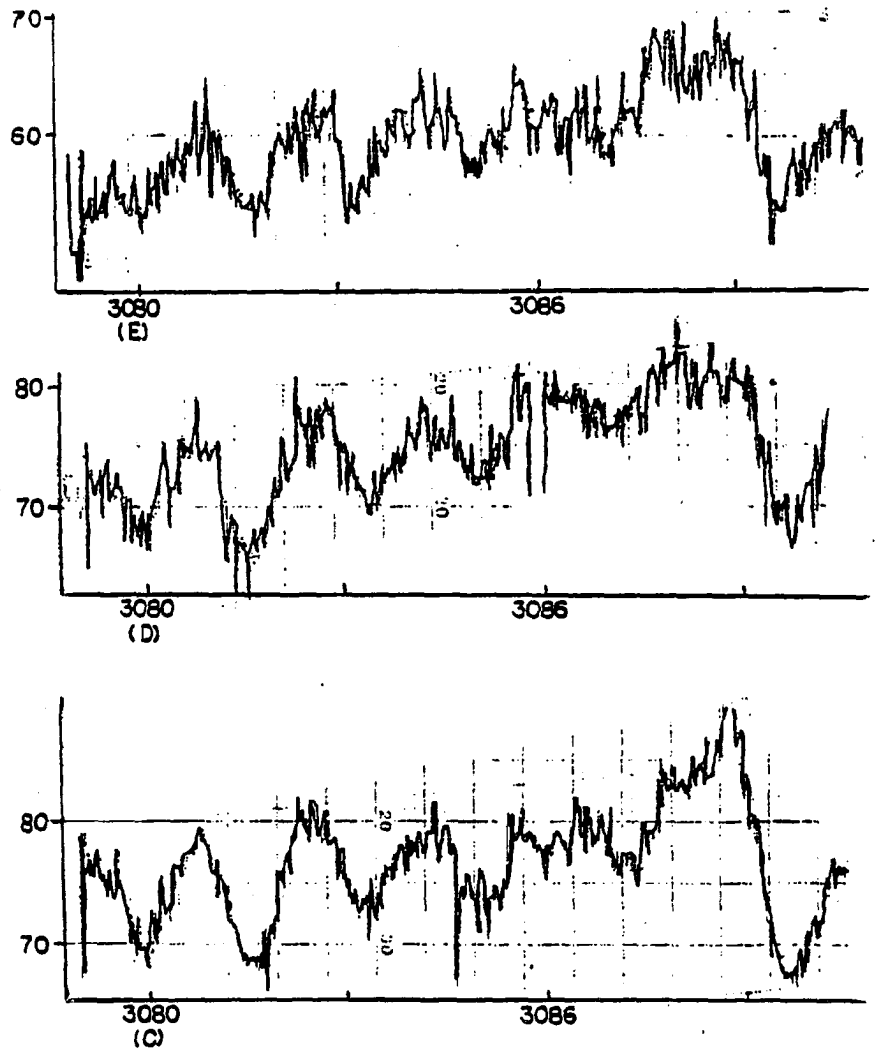

Figure 5.2, Continued. -- c) 1.77 cm above bottom flange (4j); d) 1.87 cm above bottom flange (4h); e) 1.96 cm above bottom flange (4n).

Figure 5.3 illustrates the placement of line center for the transitions studied. Overlapping lines are included. The vertical scale indicates relative magnitudes of rotational line strengths.

The peak absorption for each transition was determined as the ratio of the deviation from the baseline to the height of the baseline. The height of the baseline was the difference between the voltages (as represented on the strip chart recorder) corresponding to 100 percent absorption and 0 percent absorption. The point of 100 percent absorption was determined by covering the output of the optical fibers. The point of 0 percent absorption was determined from nonabsorbing segments of the spectra. The peak absorption measured was taken from the spectra at a point corresponding to the transition's line center, i.e., 3080.0 Å, 3081.5 Å, etc.

In the case of noisy signals, the baseline and absorption lines were drawn by "eyeball fit" to the spectra. Figure 5.4, representing the unattenuated light intensity at experimental conditions similar to those in actual absorption runs, served as a guide. The baseline is seen to have an upward drift with increasing wavelength. This is due to increases of responsivity of the photomultiplier tube (pmt) and lamp intensity with increasing wavelength.

For 40 μm slits, the recorder trace returns to the baseline representing 0 percent absorption at segments between the transitions. This was not the case with 50 μm slits, and the baseline had to be approximated. In this instance, the spectral region around 3089 Å, which is free from absorbing transitions, was used as an indication of 0 percent absorption. Typical operating conditions resulted in a

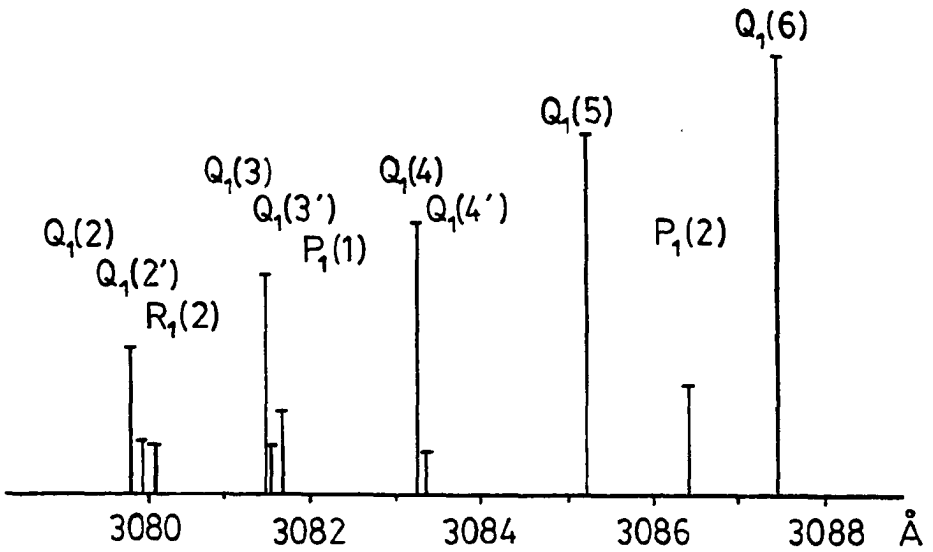

Figure 5.3 Line analysis of OH transitions in region of λ = 3080 Å to λ = 3088 Å.

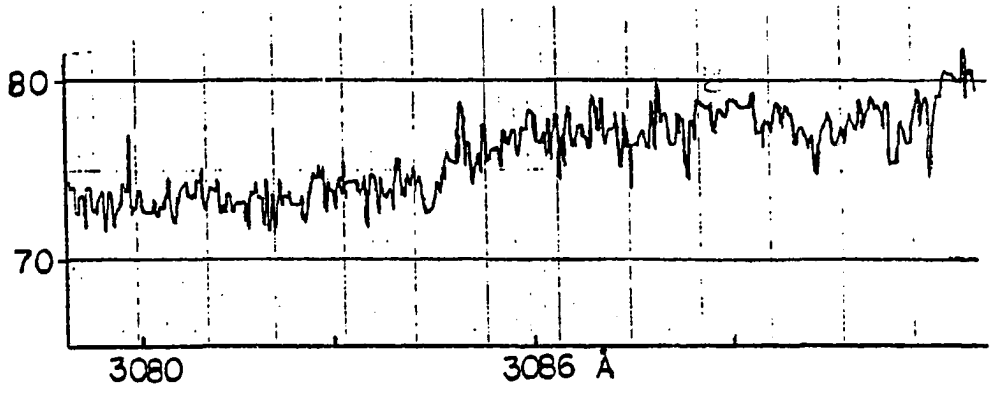

Figure 5.4 Unattenuated lamp intensity.

baseline with a positive slope of 0.1 cm/Å. Unless circumstances warranted another approach, the baseline was drawn in this way.

The peak absorptions at each absorbing wavelength were averaged over the scans at each placement. A computer program was written for use on a laboratory microcomputer to calculate OH concentrations from peak absorptions. The computational procedure follows Chapter 3 and is listed in Appendix C. Overlapping lines were taken into account in the calculation by applying the wide slit approximation to overlapping lines at the same time. The resulting concentrations corresponding to each transition were then averaged. The results for each placement in the flame are summarized in Table 5.1.

An emission spectrum of the studied flame is presented in Figure 5.5. The spectrum was taken at a sensitivity exceeding that of the absorption experiments. The spectrum was taken at a plane in the active combustion region, where OH was thought to be at about maximum. It is seen that the assumption that emission from the flame was negligible was accurate, as no emission at any transition is evident.

Premixed flame data are presented in Table 5.2. The equilibrium OH concentration corresponding to fuel/oxidant mixture and measured temperature was calculated by a computer program in use in our laboratory. The discrepancy between experimentally determined OH and equilibrium OH is quite large. However, the equilibrium OH seems to be quite low, and the experimentally determined OH is probably more accurate. Experimental difficulties associated with attaining a stable flame were considerable. Air flows from a compressor in the building were not constant. The system was not airtight, and air entrainment most likely was an

Table 5.1 Summary of experimental data for $CO/H_2/He$ vs. O_2/He opposed-jet diffusion flame.

Height above Bottom Flange (±0.03 cm)	Temperature (±20 K)	Concentration	
		10^{15} molecules/cm^3	ppm
2.15	1468	3.05	612
2.09	1541	2.56	538
1.99	1638	4.39	979
1.95	1695	5.92	1367
1.92	1680	4.77	1093
1.87	1655	6.40	1444
1.83	1640	5.92	1323
1.80	1630	7.22	1603
1.79	1620	6.47	1429
1.77	1610	6.80	1492
1.71	1580	6.82	1469
1.67	1565	6.47	1381
1.63	1540	6.75	1416
1.62	1535	4.97	1040
1.55	1490	5.64	1146
1.53	1470	5.09	1019
1.44	1435	3.09	605
1.41	1400	4.23	807
1.29	1330	2.68	486

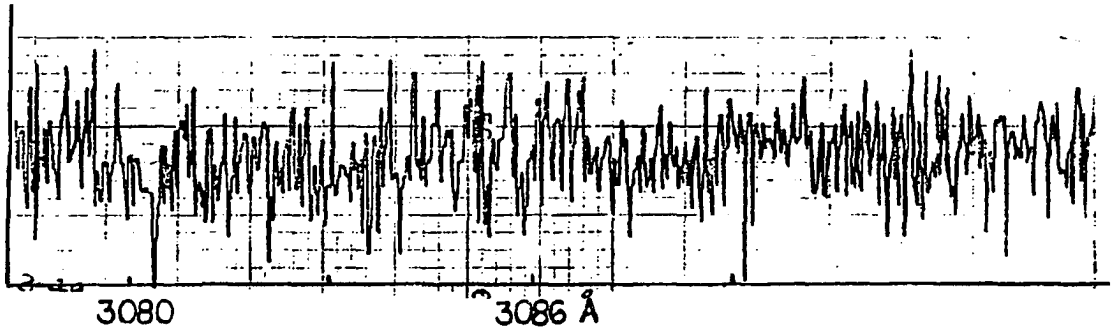

Figure 5.5 Emission spectrum of OH in region λ = 3080 Å to λ = 3088 Å.

Table 5.2 Summary of experimental data for premixed CH_4/air flame.

Temperature (±20 K)	Experimental Concentration		Equilibrium OH	
	10^{15} molecules/cm^3	ppm	10^{15} molecules/cm^3	ppm
1950	8.19	2176	0.519	138
1885	10.40	2681	2.28	586

effect. In addition to these, the path the light took through the flame was not well-defined, and possibly traversed regions where "radical overshoot" was occurring. At any rate, the purpose of experimentation with the premixed flame was to work out any bugs with the system before it was used in the opposed-jet system.

5.2 Error Analysis

Sources of error may be experimental or theoretical in nature. The latter, which include the accuracy of spectroscopic constants, the weak-line approximation, and the wide-slit approximation, are believed to contribute relatively small errors compared to experimental sources of error. Theoretical sources of error contribute mainly to errors in calculation of absolute concentrations, and have a smaller effect on relative concentrations.

Inaccurate determination of the baseline, which is a definite possibility, is one of the larger sources of experimental error. At the same time, inaccuracy of determining the peak attenuation also may contribute to an erroneous calculation of peak absorption. It is presumed that the baseline could always be drawn to within 10 percent of the true baseline and the peak attenuation determined to within 5 percent, which was essentially the noise level. The calculation of peak absorption may be written:

$$\frac{[(I_0 + \varepsilon_1) - (I + \varepsilon_2)]}{(I_0 + \varepsilon_1)} \qquad (5.1)$$

where ε_1 is the error associated with baseline determination and ε_2 is the error associated with the determination of peak attenuation. The maximum error may be derived as:

$$\frac{(\varepsilon_1 + \varepsilon_2)}{(I_0 - \varepsilon_1)} \approx 17\% \qquad (5.2)$$

The error in temperature determined by thermocouple measurement is ±20 K. Also, the accuracy of spatially positioning the thermocouple is ±0.3 mm. From the temperature profile, it is seen that the temperature gradient is on the order of 100 K/mm. This results in an overall error of ±50 K. The calculation of OH concentration specific to the Boltzmann distribution is not especially sensitive to temperature, as the total number of OH molecules in rotational states J = 2 through J = 6 will be relatively unaffected by a change in temperature. Another effect is in the calculation of gas density by the ideal gas law. The effect of temperature error on calculated concentration was determined directly by plugging temperatures into the computer program. A 50 K deviation leads to a maximum 5 percent error in calculated concentration.

To determine the error involved in the spatial positioning during absorption scans, the concentration profile is considered. The maximum gradient is approximately 250 ppm/mm. A spatial measurement of ±0.03 cm results in a possible error of 75 ppm over this range, or a relative error of 15 percent at low concentrations to a relative error of 5 percent at high concentrations.

The relative error in OH measurement arising from all experimental sources is the sum of these relative errors, and is between 30 and 40 percent.

5.3 Discussion

Results from experiments described in this thesis and from predictions of the model for a similar, but not identical, flame are depicted in Figure 5.6. It is seen that the experimental temperature and concentration profiles compare well with the predicted profiles, and data scatter is well within the 40 percent experimental error. However, a lower peak concentration, a shift in concentration from maximum temperature towards the oxidant side, and a wider concentration profile are evident. The [OH] shift was expected, and has been described in previous literature.

The region the absorbed light traversed was determined to ±0.03 cm. A cathetometer was sighted on the center of the orifices of the light baffles. The vertical adjustments on the five-axis micropositioners were set in order for the orifices to be in the same plane. Since optical adjustments were made to the point of maximum efficiency, it was fairly certain that the arc image, where maximum light intensity is, was centered within the baffles and that the light path was level.

The absorption measurements represent an integral of absorption over the space the measurements were taken. It may be assumed that the concentration profile and the temperature profile were linear over the limited vertical region studied (apparent spatial resolution is about 2 mm). If this is the case, experimentally determined [OH] represents the average concentration, and is equal to the concentration at the measured center point.

The assumption of linear concentration profile is least valid at peak absorption, i.e., the top of the profile. Obviously, the finite

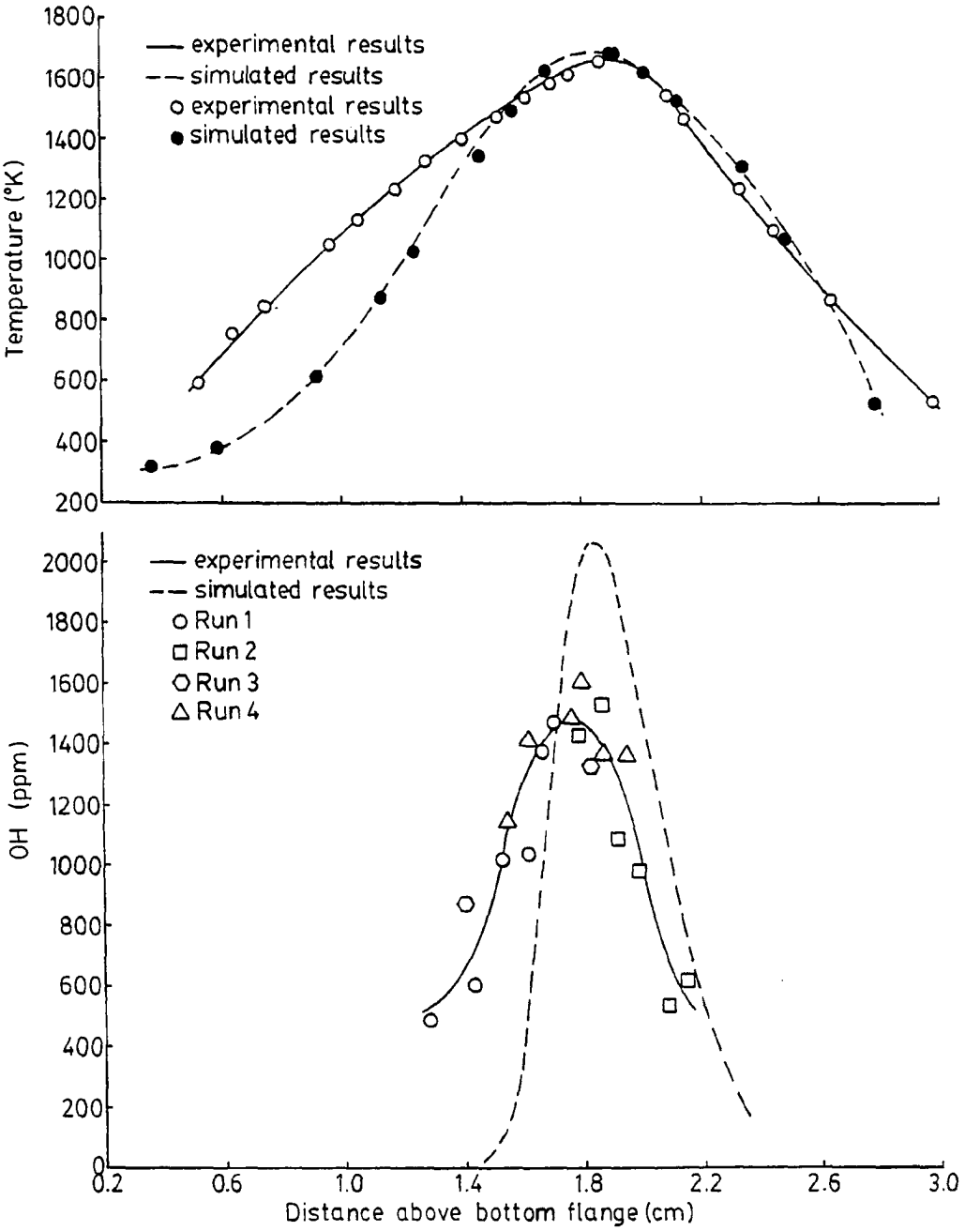

Figure 5.6 Comparison of experimentally determined [OH] and temperature with predicted [OH] and temperature.

sample volume of the beam results in a lower measured [OH] than actually exists at the point of peak concentration. In this case, it is possible that the predicted results from the simulation would match up quite well with an experimentally determined point measurement.

Visual inspection of the flame indicates that its one-dimensionality decreases with approach to the top burner. Near the top burner, edge effects occur and result in a thickening of the flame zone. Since absorption is a "line-of-sight" technique, it is possible the edge effects would lead to inaccurate measurements. Originally, it was intended to use a "probe" inserted in the flame past the edge effects to a point of homogeneity. Probes of this sort have been used in flames to get more accurate spatial resolution approaching point measurements which are generally not possible with line-of-sight techniques. Fissan and Pfender (1973) used a cooled, fiber optic probe to restrict the volume over which absorption and emission measurements were taken in a premixed flame in order to make the assumption of homogeneity. Kimball-Linne et al. (1982) also used a cooled probe for laser-induced fluorescence and absorption measurements.

Initial design of the optical system included uncooled, ceramic tubes which would be inserted into the flame through which an unattenuated light beam would travel. It was assumed that the wall destruction rate of OH radicals would be high at high temperatures, and the OH concentration inside the tube (with inner diameter 1.5 mm) would contribute negligibly to the measured absorption.

It was determined visually that edge effects were not significant in the area measurements were taken. This notion was verified with

temperature measurements. Temperature profiles were taken at radial positions to r = 0.5R and were constant. Isothermality probably exists over most of the path length.

Further evidence supportive of this assumption was seen in absorption experiments. Higher in the flame (about 2 cm above the bottom flange), where the flame is widening, Schlieren-type effects due to temperature gradients cause beam deflection, resulting in loss of signal. It was much more difficult to realign the optics in this case than it was in the case of thermal expansion of the yoke apparatus. Thermal gradients are indicative of edge effects. As stated, they were more noticeable high in the flame, where [OH] was decreasing to the point of minimum sensitivity.

Edge effects contribute most significantly at low [OH]. As a "worst case" approximation, it is supposed the light beam travels through the entire concentration gradient at the edge of the flame. (Obviously, the light beam will travel through less of the gradient at planes in the flame with high OH, and more of the gradients at planes with low OH concentrations.) To approximate this condition, the concentration gradient is assumed to have a triangular shape. Therefore, the average [OH] the light beam will see in the edge is $\frac{1}{2}$ $[OH]_{max}$ (750 ppm), and the path length is the width of the [OH] profile at $\frac{1}{2}$ $[OH]_{max}$ (0.6 cm). It follows that the relative contribution from the edge effects to measured absorption may be approximated as the ratio of the produce of average [OH] and path length in the edge [750 ppm · (2)(0.6 cm) = 900 ppm-cm] to the product of [OH] and path length in the homogeneous region. At worst, the contribution is

900/(500 · 10) ≈ 20 percent. At maximum [OH], the contribution is three times less. The effect of the edge contribution is to make the measured [OH] wider. Therefore, the true [OH] profile probably is narrower, especially at lower concentrations.

Another method of dealing with edge effects is the Abel inversion technique. It is a mathematical technique which has been used to determine the radial profiles of absorbers and emitters in axially symmetric sources. The method requires a number of scans at different horizontal placements. Considerable redesign of the optical/combustion system would be necessary for implementation of this method to be feasible.

The evolution of the optical system from a dual-beam experiment with subtraction of flame emission and electronic noise to a single-beam experiment with analog averaging to reduce noise was discussed in Chapter 4. Further discussion is in order here.

It has been shown, in this case, that flame emission is negligible. This does not imply that there are not emitters in the flame. The optical system does not efficiently collect light from the flame, but was designed to see only light from the lamp. In emission experiments, lenses are used to collect light from the flame and focus it on to the detector. The fact that flame emission need not be considered precluded use of the chopper.

The demise of the silicon photodetector was not unfortunate from an experimental point of view. The lamp, when performing within specifications, was stable enough for a single-beam experiment. Occasional increases and decreases in intensity from the lamp were evident in the

spectra. However, the duration of these deviations was short compared with the time of an absorption scan over a transition. Actually, the photodetector was not being used "correctly" in the sense of a dual-beam experiment, where its primary purpose is to indicate I_0. For this, the wavelengths of light incident on the photodetector should be the same as the wavelengths which are being absorbed. This condition may be approximated by the use of a narrow bandpass filter. This was the original intent. However, the intensity of light which was reflected off the quartz flat transmitted through a filter with a 15-nm bandpass centered at 305 nm was not enough to cause a response in the photodetector. Also, the sensitivity of the photodetector and photomultiplier tube should be equal, i.e., they should respond equally to equal changes in light intensity. This condition was approximated, but never achieved. The primary function of the photodetector in our optical system was the generation of gating signals for integration.

Finally, and pragmatically most important, the substitution of a signal generated for the photodetector and the non-use of the chopper resulted in a better signal-to-noise ratio and less baseline drift.

CHAPTER 6

RECOMMENDATIONS

The laminar, opposed-jet diffusion flame is definitely amenable to spectroscopic studies. Simplification of the experimental procedure was aided by its relatively long and homogeneous path length for absorption measurements, and the stability of the flame.

The combustion system, however, was not designed with optical studies in mind. Generally, the optics are set and the system to be studied is moved. The reverse was necessary in this study. Also, access to the optics, which was not available, definitely helps.

The simplest way to get around this problem is to reflect the light beam from the lamp off a mirror mounted on a five-axis micropositioner. When realignment is necessary, the micropositioner could be finely adjusted. The most elegant solution would be a scale-down of the combustion system to the point where it could be moved. The proposed system would have fused silica or sapphire windows for optical access. The entire combustion system would then be mounted on a table providing horizontal and vertical movement. Abel inversion techniques could be used to reduce the data. Thermocouple and sample probes could be mounted on a vertical rod extending through the bottom of the outer cylinder. Rotation of the rod would result in measurements at any radial position.

The optical system could be improved considerably. A synchronous D.C. motor with its speed controlled by a signal generator should be used. This would eliminate the problem of baseline drift due to variation in chopping speed and reduce electronic noise generated by the chopping motor. With the optics outside the combustion system, conventional lenses and mirrors could be used to increase the light efficiency. Long-focal-length lenses may be used to narrow the beam and focus it at the center of the flame. An improvement in spatial resolution would result. With no attenuation of light due to fiber optics or inefficient coupling of light to the monochromator, and improved management of light, spectral resolution could also be improved. For example, in the premixed flame system, with which access to the optics was available, there was enough light incident on the pmt to narrow the slits to 35 μm, even with the fiber optics relay.

The arc lamp is adequate and has its advantages, which were discussed in Chapter 4. An improvement of the background radiation source would be the use of a tunable, ultraviolet laser. The monochromator and photomultiplier tube and its power supply are also adequate.

The detection electronics could be improved considerably by implementation of phase-sensitive detection, i.e., lock-in amplification. Modules for this purpose may be purchased from the same manufacturer as the gated integrators were. While a homemade system with these modules would be a fraction of the cost of off-the-shelf, lock-in amplifiers, it is suggested that, unless one is experienced with electronics and is knowledgeable of experimental techniques, the unit be purchased off-the-shelf.

The output from the amplifier(s) may be sent to an a/d conversion board, which will soon be in use in our laboratory computer. Rapid data point averaging would result in a much less noisy signal.

Off-the-shelf software for analysis of spectroscopic data is available from many manufacturers. With the advent of widespread usage of laboratory micro- and mini-computers, recent publications have dealt with the subject of smoothing of spectroscopic data (Bromba and Ziegler, 1981; Kawata and Minami, 1984; Snyder and Hooker, 1984).

APPENDIX A

SPECTROSCOPIC AND OTHER CONSTANTS

Table A.1 Spectroscopic constants.

Planck constant	h	6.628×10^{-34} J sec
Boltzmann constant	k	1.381×10^{-23} J K^{-1}
Speed of light	c	2.998×10^{10} cm sec^{-1}
Band oscillator strength	$f_{v''v'}$	9.0×10^{-4}*
Rotational constant	B_e	18.52 cm^{-1}*
Vibrational constant	ω_e	3739.94 cm^{-1}*

*For $^2\pi$ state of OH, $v'' = 0$, $v' = 0$.

Table A.2 Other constants.

Analysis	ν (cm^{-1})	$T_{J"J'}$	$S_{J"J'}$
$Q_1(2)$	32,458.7	0.994	17.0
$Q_1(3)$	32,441.9	0.990	25.3
$Q_1(4)$	32,423.6	0.984	33.7
$Q_1(5)$	32,403.5	0.978	42.2
$Q_1(6)$	32,381.0	0.969	50.6

APPENDIX B

RAW DATA

Table B.1 Run #1, 50 μm slit width.

Designation	Δz (cm)	Maximum Fractional Absorption				
		$Q_1(2)$	$Q_1(3)$	$Q_1(4)$	$Q_1(5)$	$Q_1(6)$
1a	1.53	0.100	0.078	0.043	0.053	0.053
1b	1.53	0.082	0.096	0.059	0.085	0.076
1c	1.53	0.079	0.106	0.066	0.087	0.091
1d	1.53	0.082	0.097	0.063	0.101	0.003
1e	1.44	0.069	0.080	0.045	0.022	0.055
1f	1.44	0.030	0.042	0.042	0.042	0.058
1g	1.29	0.062	0.061	0.017	0.049	0.032
1h	1.67	0.120	0.124	0.112	0.077	0.060
1i	1.67	0.114	0.136	0.106	0.082	0.065
1j	1.67	0.088	0.110	0.086	0.056	0.056
1k	1.71	0.096	0.095	0.082	0.058	0.074
1l	1.71	0.121	0.120	0.113	0.106	0.100
1m	1.62	0.073	0.096	0.071	0.071	0.070
1n	1.62	0.078	0.091	0.072	0.048	0.065

Table B.2 Run #2, 50 μm slit width.

Designation	Δz (cm)	Maximum Fractional Absorption				
		$Q_1(2)$	$Q_1(3)$	$Q_1(4)$	$Q_1(5)$	$Q_1(6)$
2a	1.87	0.086	0.067	0.067	0.065	0.091
2b	1.87	0.102	0.110	0.094	0.092	0.097
2c	1.87	0.129	0.105	0.098	0.120	0.107
2d	1.79	0.114	0.105	0.079	0.090	0.094
2e	1.79	0.105	0.123	0.078	0.083	0.071
2f	1.66	0.123	0.117	0.079	0.090	0.112
2g	1.66	0.096	0.100	0.086	0.110	0.084
2h	1.92	0.068	0.087	0.080	0.072	0.091
2i	1.92	0.055	0.075	0.094	0.067	0.053
2j	1.92	0.045	0.074	0.067	0.079	0.057
2k	1.99	0.074	0.058	0.044	0.064	0.082
2l	1.99	0.045	0.060	0.051	0.072	0.078
2m	1.99	0.030	0.074	0.073	0.065	0.078
2n	2.09	0.010	0.058	0.029	0.043	0.044
2o	2.09	0.010	0.045	0.045	0.037	0.059
2p	2.15	0.034	0.052	0.051	0.051	0.050
2q	2.15	0.031	0.050	0.044	0.050	0.060

Table B.3 Run #3, 50 μm slit width.

Designation	Δz (cm)	Maximum Fractional Absorption				
		$Q_1(2)$	$Q_1(3)$	$Q_1(4)$	$Q_1(5)$	$Q_1(6)$
3a	1.41	0.060	0.093	0.070	0.046	0.074
3b	1.41	0.061	0.096	0.048	0.059	0.070
3c	1.62	0.072	0.094	0.046	0.064	0.068
3d	1.62	0.086	0.097	0.074	0.057	0.091
3e	1.72	0.090	0.102	0.060	0.073	0.098
3f	1.72	0.133	0.118	0.117	0.090	0.139
3g	1.83	0.110	0.090	0.051	0.075	0.074
3h	1.83	0.082	0.116	0.068	0.093	0.092
3i	1.83	0.082	0.116	0.068	0.074	0.080
3j	1.92	0.045	0.045	0.051	0.064	0.051
3k	1.92	0.052	0.058	0.071	0.096	0.051
3l	1.92	0.080	0.045	0.058	0.083	0.101

Table B.4 Run #4, 40 μm slit width.

Designation	Δz (cm)	Maximum Fractional Absorption				
		$Q_1(2)$	$Q_1(3)$	$Q_1(4)$	$Q_1(5)$	$Q_1(6)$
4a	1.63	0.123	0.150	0.135	0.135	0.099
4b	1.63	0.133	0.144	0.116	0.096	0.119
4c	1.63	0.116	0.160	0.134	0.146	0.106
4d	1.80	0.125	0.159	0.103	0.136	0.135
4e	1.80	0.154	0.186	0.105	0.117	0.121
4f	1.80	0.139	0.150	0.099	0.110	0.048
4g	1.87	0.133	0.171	0.130	0.115	0.075
4h	1.87	0.118	0.135	0.077	0.063	0.100
4i	1.55	0.135	0.156	0.130	0.153	0.128
4j	1.77	0.136	0.146	0.114	0.132	0.099
4k	1.80	0.155	0.155	0.125	0.111	0.116
4l	1.88	0.106	0.139	0.102	0.093	0.105
4m	1.88	0.114	0.120	0.095	0.101	0.092
4n	1.96	0.090	0.103	0.122	0.092	0.090
4o	1.94	0.134	0.134	0.103	0.088	0.080
4p	1.94	0.132	0.147	0.103	0.109	0.080

APPENDIX C

COMPUTATIONAL PROCEDURE

```
      PROGRAM CONC
      DIMENSION PPMV(6),FACT(6),FROT(6),CORR(6),STREN2(6)
      DIMENSION ABSMAX(6),ABSCON(6),ENERGY(6),STRENG(6)
C
C     PROGRAM CONC CALCULATES OH CONCENTRATION FROM PEAK ABSORPTION
C     MEASUREMENTS FROM TRANSITIONS Q1(2),Q1(3),Q1(4),Q1(5),Q1(6).
C     ITS OUTPUT IS IN [CM-3] AND [PPM].THE PROGRAM STORES SPECTROSCOPIC
C     DATA I.E. ROTATIONAL AND VIBRATIONAL CONSTANTS,TRANSITION PROB-
C     ABILITY,OSCILLATOR STRENGTHS,AND CONSTANTS NECESSARY FOR CALCULA-
C     TION OF [OH] AS PER CHAPTER THREE.
C
      DATA STRENG,FROT,CORR,OSC,CONST1,CONST2/0.0,17.0,25.3,33.7,
     *42.2,50.6,0.0,83.7,201.9,355.1,543.5,767.5,0.0,.994,.990,.984,
     *.978,.969,9.E-4,1.44,4.52E12/
      DATA RMOL/82.0575/,YES/1HY/
      DATA STREN2/0.0,5.1,5.3,4.9,4.4,4.0/
C
  500   CONTINUE
      WRITE(3,1000)
C
C     THE PROGRAM ASKS THAT TEMPERATURE,SPECTRAL SLIT WIDTH,OPTICAL
C     PATH LENGTH,PLACEMENT IN FLAME,AND MEASURED PEAK ABSORPTION BE
C     ENTERED BY THE KEYBOARD
C
 1000 FORMAT(/,5X,'ENTER TEMPERATURE (K)')
      READ(3,100)T
        WRITE(3,3001)
 3001   FORMAT(/,5X,'ENTER DISTANCE FROM TOP FLANGE (CM)')
        READ(3,100)Z
      WRITE(3,1001)
 1001 FORMAT(/,5X,'ENTER SLIT WIDTH (CM-1)')
      READ(3,100)DELWAY
      WRITE(3,1002)
 1002 FORMAT(/,5X,'ENTER OPTICAL PATH LENGTH (CM)')
      READ(3,100)PATHLN
      DO 1 J=1,6
          WRITE(3,1003)J
 1003     FORMAT(/,5X,'ENTER MAXIMUM ABSORPTION(',I2,')')
          READ(3,100)ABSMAX(J)
   1  CONTINUE
C
C     CALCULATE ROTATIONAL AND VIBRATIONAL PARTITION FUNCTIONS
C
      BV=18.52
      QROT=3.96*T/(CONST1*BV)
      QVIB=1.0/(1.-EXP(-CONST1*3739.94/T))
C
C     ELIMINATE G(VIB) SINCE THE SAME VIBRATIONAL QUANTUM NUMBER
C     IS PRESENT FOR THE TRANSITION EXAMINED EXPERIMENTAL.
```

```
C
      GVIB=0.0
      SUM=0.0
      FACT(1)=0.0
C
C     A CORRECTION FACTOR IS APPLIED TO THIS MEASURED ABSORPTION
C     TO ACCOUNT FOR OVERLAPPING LINES
C
      FACT(2)=EXP(FROT(2)*CONST1/T)/(STRENG(2)*CORR(2)+STREN2(2)+5.7)
      FACT(3)=EXP(FROT(3)*CONST1/T)/(STRENG(3)*CORR(3)+STREN2(3)+
     *(1.09/9.4))
      DO 8 J=4,6
      FACT(J)=EXP(FROT(J)*CONST1/T)/(STRENG(J)*CORR(J)+STREN2(J))
   8    CONTINUE
C
C     CALCULATE CONCENTRATION OF OH
C
      DO 2 J=2,6
          RJ=FLOAT(J)
          AK=ABSMAX(J)*DELWAY/PATHLN
          ABSCON(J)=CONST2*AK*QVIB*QROT*FACT(J)/OSC
        PPMV(J)=(ABSCON(J)/6.0225E17)*RMOL*T
        SUM=SUM+PPMV(J)/5.
   2  CONTINUE
 100  FORMAT(F10.0)
C
C     PRINT OUT EXPERIMENTAL VARIABLES AND CALCULATED [OH]
C
        WRITE(3,3000)T,Z,DELWAY,PATHLN
3000    FORMAT(//,5X,'SUMMARY:',/,15X,'TEMPERATURE=',F6.1,2X,'DEG K',
     1  /,15X,'DISTANCE FROM TOP FLANGE=',F6.3,2X,'CM',/,15X,
     2  'SLIT WIDTH=',2X,F6.3,2X,'CM-1',/,15X,
     3  'OPTICAL PATH LENGTH=',F6.3,2X,'CM')
        WRITE(3,2000)
2000    FORMAT(//,5X,'Q(J)',4X,'IMAX',8X,'CONC',11X,'PPMV')
        DO 2005 J=2,6
        WRITE(3,2001)J,ABSMAX(J),ABSCON(J),PPMV(J)
2001    FORMAT(7X,I2,5X,F5.0,3X,1PE12.4,3X,1PE12.4)
2005    CONTINUE
      WRITE(3,300)SUM
300   FORMAT(//,5X,'AVERAGE CONCENTRATION IS',2X,E11.4)
        WRITE(3,2010)
2010    FORMAT(/,5X,'ANOTHER DATA SET? (Y/N)')
        READ(3,2015)ANS
2015    FORMAT(A1)
        IF(ANS.EQ.YES)GOTO500
      END
```

REFERENCES

Anketell, J., and A. Pery-Thorne, Proc. Roy. Soc., A301, 355 (1967).

Bleekrode, R., and W. C. Neiuwpoort, J. Chem. Phys., 43, 3680 (1965).

Bromba, M., and H. Ziegler, Anal. Chem., 53, 1583 (1981).

Bulewicz, E., P. J. Padley, and R. E. Smith, Proc. Roy. Soc., A315, 129 (1970).

Corley, T. L., personal communication (1984).

Crosley, D. R., Laser Probes in Combustion Chemistry, American Chemical Society, New York (1980).

Dieke, G. H., and H. M. Crosswhite, J. Quant. Spectr. Rad. Transfer, 2, 97 (1962).

Drayson, S., J. Quant. Spectr. Rad. Transfer, 16, 611 (1976).

Fenimore, C. P., Thirteenth Symposium (International) on Combustion, The Combustion Institute, Pittsburgh (1971).

Fenimore, C. P., Comb. Flame, 26, 249 (1976).

Fissan, J. H., and E. Pfender, Int. J. Heat Transfer, 16, 991 (1973).

Gaydon, A. G., and H. G. Wolfhard, Proc. Roy. Soc., A191, 185 (1948).

Glassman, I., Combustion, Academic Press, Inc., New York (1977).

Hahn, W., and J. O. L. Wendt, Chem. Eng. Comm., 9, 121 (1981).

Hardy, A. C., and F. M. Young, J. Opt. Soc. Am., 39, 265 (1949).

Haynes, B. S., Comb. Flame, 28, 81 (1977a).

Haynes, B. S., Comb. Flame, 28, 113 (1977b).

Herzberg, G., The Spectra and Structures of Simple Free Radicals, Cornell University Press, Ithaca (1971).

Jessen, P. F., and A. G. Gaydon, Twelfth Symposium (International) on Combustion, The Combustion Institute, Pittsburgh (1969).

Kaskan, W. E., Sixth Symposium (International) on Combustion, The Combustion Institute, Pittsburgh (1957).

Kaskan, W. E., J. Chem. Phys., 31, 944 (1959).

Kawata, S., and S. Minami, Appl. Spectr., 38, 49 (1984).

Kimball-Linne, M., G. Kychakoff, R. Hanson, and R. Burman, Western States Section/Combustion Institute, Fall (1982).

Kostowski, H. J., and A. Bass, J. Opt. Soc. Am., 46, 1060 (1956).

Kostowski, H. J., and H. Broida, J. Opt. Soc. Am., 46, 246 (1956).

Laud, B. B., and A. G. Gaydon, Comb. Flame, 16, 55 (1971).

Mavrodineanu, R., and H. Boiteux, Flame Spectroscopy, John Wiley and Sons, New York (1965).

Mitchell, A., and M. W. Zemansky, Resonance Radiation and Excited Atoms, Cambridge University Press, London (1934).

Morley, C., Comb. Flame, 27, 189 (1976).

Nadler, M., and W. E. Kaskan, J. Quant. Spectr. Rad. Transfer, 10, 25 (1970).

Penner, S. S., Quantitative Molecular Spectroscopy and Gas Emissivities, Addison-Wesley, Reading, Massachusetts (1959).

Schmidt, S. C., and P. C. Malte, J. Quant. Spectr. Rad. Transfer, 16, 963 (1976).

Snyder, R. W., and T. Hooker, Appl. Spectr., 38, 58 (1984).

Steinfeld, J., Molecules and Radiation, Harper and Row, New York (1974).

Sulzmann, K., J. Quant. Spectr. Rad. Transfer, 29, 89 (1983).

Whiting, E. E., J. Quant. Spectr. Rad. Transfer, 8, 1379 (1968).

Wolfhard, H. G., and W. G. Parker, Proc. Phys. Soc. (London), A62, 722 (1949).

Wolfhard, H. G., and W. G. Parker, Proc. Phys. Soc. (London), A65, 2 (1952).

Zeldovich, Y. Acta Physecochem. (U.S.S.R.), 21, 577 (1946).